Physics – Uspekhi **48** (9) 867 – 885 (2005)

REVIEWS OF TOPICAL PROBLEMS PACS numbers: **06.20. – f**, 14.20.Dh, **28.20. – v**

Neutron lifetime measurements using gravitationally trapped ultracold neutrons

A P Serebrov

DOI: 10.1070/PU2005v048n09ABEH003536

Contents

Abstract. Experiments using gravitationally trapped ultracold neutrons (UCNs) to measure the neutron lifetime are reviewed. The precise value of the neutron lifetime is of fundamental importance to particle physics and cosmology. In our experiment, the UCN storage time is brought closest ever to the neutron lifetime: the probability of the UCN loss from the trap was only 1% of that for neutron β-decay. The neutron lifetime obtained, $878.5 \pm 0.7_{stat} \pm 0.3_{sys}$ s, is the most accurate one to date. The impact of the new result on testing the unitarity of the quark mixing matrix and on data analysis for the primordial nucleosynthesis model is scrutinized.

A P Serebrov B P Konstantinov Petersburg Nuclear Physics Institute, Russian Academy of Sciences,
188300 Gatchina, Leningrad Region, Russian Federation
Tel. (7-81371) 46 001
E-mail: serebrov@pnpi.spb.ru

Received 16 March 2005, revised 30 June 2005
Uspekhi Fizicheskikh Nauk **175** (9) 905 – 924 (2005)
Translated by E Yankovsky; edited by A Radzig

1. Introduction

The problem of precise measurements of the neutron lifetime is important for elementary particle physics and cosmology. The decay of a free neutron into a proton, an electron, and an antineutrino is determined by the weak interaction comprising the transition of a d-quark into a u-quark.

In the Standard Model of elementary particles, the quark mixing is described by the Cabibbo – Kobayashi – Maskawa (CKM) matrix which must be unitary. For instance, for the first row we have

$$|V_{ud}|^2 + |V_{us}|^2 + |V_{ub}|^2 = 1\,, \tag{1.1}$$

where V_{ud}, V_{us} and V_{ub}, are the matrix elements responsible for the mixing of a u-quark with a d-, s-, or b-quark, respectively. The values of the individual matrix elements are determined by the weak decays of the respective quarks. In particular, the matrix element V_{ud} can be determined from the data on nuclear β-decay and neutron β-decay. The extraction of V_{ud} from the data on neutron β-decay is extremely tempting due to the theoretical simplicity of describing the neutron decay compared to the description

of nuclear decay. Unfortunately, the experimental procedure is a very complicated one, since it requires precise measurements of the neutron lifetime τ_n and the β-decay asymmetry A_0. The neutron half-life t is given by the following equation [1]

$$ft(1+\delta'_R) = \frac{K}{|V_{ud}|^2 G_F^2 (1+3\lambda^2)(1+\Delta_R)}, \quad (1.2)$$

where $f = 1.6886$ is the phase space factor, $\delta'_R = 1.466 \times 10^{-2}$ is a model-independent external radiative correction calculated with an accuracy of 9×10^{-5} [2, 3], $\Delta_R = 2.40 \times 10^{-2}$ is a model-dependent internal radiative correction calculated with an accuracy of 8×10^{-4} [4, 5], λ is the ratio of the axial-vector weak coupling constant to the vector weak coupling constant, $\lambda = G_A/G_V$, G_F is the Fermi weak coupling constant determined from the μ-decay, and $K = \hbar(2\pi^3 \ln 2)(\hbar c)^6/(m_e c^2)^5$.

The general formula for calculating $|V_{ud}|^2$ on the basis of the data on neutron β-decay has the form [1, 3]

$$|V_{ud}|^2 = \frac{4908 \pm 4 \text{ s}}{\tau_n(1+3\lambda^2)}, \quad (1.3)$$

where the inaccuracy in calculations of the radiative corrections was taken into account. Thus, the required relative accuracy of measuring the neutron lifetime τ_n must be higher than 10^{-3}, while the relative accuracy of measuring λ must be higher than 0.5×10^{-3}. The parameter λ is found from measurements of the asymmetry A_0 of neutron β-decay:

$$A_0 = -2\frac{\lambda(\lambda+1)}{1+3\lambda^2}. \quad (1.4)$$

Since $\Delta\lambda/\lambda = 0.25\Delta A_0/A_0$, the relative accuracy of measuring the A-asymmetry must be higher than 2×10^{-3}. At present, the relative accuracy of measuring A_0 amounts to 6×10^{-3} ($A_0 = -0.1189(7)$ [6]), while the relative accuracy of measuring τ_n is 8×10^{-4} ($\tau_n = 885.7(7)$ s [7]). The value of $|V_{ud}|$ obtained with these values equals 0.9717(13).

The matrix element V_{us} can be extracted from the decays of strange particles, hyperons, and K-mesons. In the Particle Data Group tables, the current value is $|V_{us}| = 0.2196(23)$ [7], but a recent analysis of the data [8] yields $|V_{us}| = 0.2272(30)$. The matrix element $|V_{ub}| = 0.0037(5)$ [7] provides a negligible contribution to the test of the unitarity of the CKM matrix. Thus, with the Particle Data Group data for V_{us}, the sum of the squares of the matrix elements from the first row of the CKM matrix is given by [1]

$$|V_{ud}|^2 + |V_{us}|^2 + |V_{ub}|^2 = 1 - \Delta = 0.9924(28), \quad (1.5)$$

where $\Delta = 0.0076(28) = 2.7\sigma$. The deviation from unitarity by 2.7 standard errors is certainly important and requires detailed analysis from both the experimental and theoretical viewpoints.

The accuracy of experiments in determining the neutron lifetime is high enough: the accuracy of the world average of τ_n amounts to one part in a thousand; prior to 2004, the highest accuracy achieved in experiments was that of Arzumanov et al. [9]. The accuracy of experiments on the asymmetry of neutron decay, which is lower than the accuracy of experiments on measuring the neutron lifetime, determines the error in V_{ud}. Of course, it is extremely important to raise the accuracy of determining the parameter λ from measurements of the neutron decay asymmetry by a factor of four to five. However, new experiments on measuring the neutron lifetime are also needed.

The violation of the unitarity of the CKM matrix means that we have gone beyond the Standard Model comprising three generations of quarks and leptons. The scope of theoretical models based on extensions of the Standard Model is reasonably broad: they include the possibility of increasing the number of generations [10, 11], and the existence of an additional Z-boson [12, 13] as well as right-handed currents in weak interactions [14]. Hence, precise experiments examining neutron β-decay are highly important, especially in connection with the above-noted discrepancy at the 2.7σ level.

Precise measurements of the neutron lifetime are also critically important when one wishes to verify a model of the early stages of the formation of the Universe. In the Big Bang model, at a temperature $T > 10^{10}$ K ($E > 1$ MeV), the leptons, hadrons, and photons are in a state of thermodynamic equilibrium. As $T < 1$ MeV, neutrinos are already incapable of sustaining this equilibrium state, since the rate of weak processes drops below the rate at which the Universe expands. The ratio N_n/N_p of the number of neutrons to the number of protons at such a temperature is determined by the Boltzmann factor, $N_n/N_p = \exp(-\Delta m/T_f)$, where Δm is the difference in the neutron and proton masses, and T_f is the temperature at which weak-interaction reactions are frozen. Subsequently, the fraction of neutrons further decreases because of neutron β-decay. The nucleosynthesis process leads to the formation of deuterium and helium, mainly ^{4}He. The abundance of these elements is determined by the ratio N_n/N_p. The key parameter that makes it possible to estimate the nucleosynthesis effect is the number of baryons per photon, $\eta_{10} = N_b/N_\gamma$. This parameter is related to the temperature and density of the early Universe and makes it possible to determine the conditions in which nuclear synthesis occurs. From this one can derive the initial element abundance. The following factors must be included in calculations of the nucleosynthesis of light elements: the rate $\Gamma_w = (7/60)\pi(1+3\lambda^2)G_F^2 T^5$ of weak reactions, the rate of expansion of the Universe, the baryon asymmetry η_{10}, and the neutron lifetime τ_n. Actually, the neutron lifetime enters the problem twice. It determines the rate of weak-interaction processes (the shorter the neutron lifetime, the faster weak reactions proceed and the earlier the neutrinos leave the state of thermodynamic equilibrium). In addition, a shorter neutron lifetime will produce fewer neutrons in the period when weak interactions become frozen and nuclear synthesis begins.

The observed quantities in the Big Bang model are the initial abundances of deuterium and ^{4}He. These depend on the ratio of the number of baryons to the number of photons in the initial nucleosynthesis stage and on the neutron lifetime τ_n. For instance, at a fixed value of η_{10}, a variation in the neutron lifetime by 1% changes the value of the initial abundance of ^{4}He by 0.75%. The relative accuracy of measurement of the helium-4 abundance comprises ±0.61% [15]. Similarly, a variation in the neutron lifetime by 1% changes η_{10} by 17%, although the modern accuracy of estimation of this quantity amounts to ±3.3% [15]. Thus, to verify the nucleosynthesis model in the Big Bang, the accuracy of measuring the neutron lifetime must be higher than 1%.

2. Experiments on measuring the neutron lifetime

All experiments on measuring the neutron lifetime can be divided into two groups: beam experiments, and neutron-storage experiments. In experiments of the first type, the measured quantity is the rate of neutron decay inside a selected region of a neutron beam. The neutron lifetime τ_n is found from the equation

$$\frac{dN}{dt} = -\frac{N}{\tau_n}, \tag{2.1}$$

where N is the number of neutrons, and dN/dt is the rate with which the products of neutron decay (electrons or protons) appear in the decay region. Note that beam experiments require absolute measurements of both the number of neutrons and the rates of neutron decay in the decay region.

Experiments on measuring the neutron lifetime that use the neutron-storage method are based on the solution of equation (2.1):

$$N(t) = N(0)\exp\left(-\frac{t}{\tau_n}\right), \tag{2.2}$$

where $N(0)$ is the number of neutrons captured by a trap at instant $t = 0$, and $N(t)$ is the number of neutrons that remain in the trap by time t.

When the neutrons are stored in material traps, formula (2.2) should be written as follows

$$N(t) = N(0)\exp\left[-t\left(\frac{1}{\tau_n}+\frac{1}{\tau_{loss}}\right)\right], \tag{2.3}$$

where $1/\tau_{loss}$ is the probability of neutron losses as the neutrons interact with the trap walls.

Solving equation (2.3) in $1/\tau_n$ yields

$$\frac{1}{\tau_n} = \frac{\ln\left(N(0)/N(t)\right)}{t} - \frac{1}{\tau_{loss}}. \tag{2.4}$$

The quantity $1/\tau_{loss}$ can be found by the size or energy extrapolation method. Since relationship (2.4) contains only the ratio of the numbers of neutrons in the trap at different instants of time, the given method has an important advantage, and that is the relative nature of measuring the number of neutrons in the trap. This advantage makes it possible to avoid an entire range of systematic errors which are inherent in the beam methods applied to determining the neutron lifetime.

The first experiment on measuring τ_n with an accuracy higher than 10 s by recording the decay protons was conducted by P E Spivak and co-workers at the Kurchatov Institute of Atomic Energy, Moscow [16]. The first beam experiment in which the decay electrons were recorded was conducted by C J Christensen et al. [17].

The most accurate experiment of the beam type was conducted in 2003 at the National Institute of Standards and Technology, Gaithersburg, USA. The experimenters recorded the decay protons that accumulated in the decay region of the beam, utilizing a Penning trap. In such a trap (a long solenoid with a 4.6-T magnetic field), the decay protons move along small-radius helixes that 'wind' around the lines of force of the magnetic field. An electrostatic field directed along the solenoid's axis blocked the protons. After a certain accumulation period, the electrostatic barrier was lifted and the blocked protons were recorded by a semiconductor detector. The flux of cold neutrons through the decay region was measured by a method in which the neutrons were first captured in a thin ^{6}LiF layer and then the alpha particles and tritons were recorded. The experiment yielded the following value $886.8 \pm 1.2_{stat} \pm 3.2_{sys}$ s [18] for the neutron lifetime τ_n. The systematic error in this experiment is determined by the errors in finding the mass of the ^{6}LiF deposit and the cross section of the reaction of neutron capture by the ^{6}Li isotope.

The possibility of storing ultracold neutrons and measuring their lifetime by such a method was first mentioned by Ya B Zel'dovich in 1959 [19]. The first experiment on measuring the neutron lifetime by the UCN storage method was conducted by V I Morozov in 1985 at the Atomic Reactor Research Institute in Dimitrovgrad (Russia). Later, a more accurate experiment that used the neutron storage method was conducted at the Institut Laue–Langevin (ILL) in Grenoble (France) by Morozov's group from the Kurchatov Institute of Atomic Energy (see Ref. [9]). In this experiment, the UCNs were retained in an aluminium trap whose walls were covered by a layer of Fomblin, a hydrogen-free oil. The neutron trap consisted of two horizontal cylinders with one inside the other. The ultracold neutrons could be stored either inside the inner cylinder or in the gap between the two cylinders. Thus, the experimenters were able to vary the UCN mean free path prior to collisions with the walls and, hence, the neutron loss at the walls. The mean value of the UCN loss probability in relation to neutron β-decay probability in this experiment amounted to about 30%. The losses at the trap walls were not calculated. Instead, another method was used, a method based on allowing for the fact that the UCN loss at the trap walls is proportional to the flux of thermal neutrons that were inelastically scattered by the walls and acquired an energy close to thermal. To register the inelastically scattered neutrons, the UCN trap was surrounded by counters of thermal neutrons. However, there was a certain price to pay for such an original approach: one had to know with high accuracy the ratio of the efficiencies of registering thermal neutrons and UCNs for different configurations of the UCN trap. As a result of this experiment, the neutron lifetime was found to be equal to $885.4 \pm 0.9_{stat} \pm 0.4_{sys}$ s [9]. The systematic error of the experiment was conditioned by the error in determining the efficiencies of registering thermal neutrons in the course of storing UCNs in the gap and in the inner cylinder.

Figure 1 and Table 1 give the results of experiments on measuring the neutron lifetime. Keeping only those results whose accuracy is higher than 10 s, the Particle Data Group calculated the average value of the neutron lifetime, and reported 885.7(8) s [7].

In Sections 3–6, I describe in detail our experiment that uses a gravitational UCN trap, with which the closest approximation of the UCN storage time to the extrapolated value of the neutron lifetime was achieved. The probability of the UCN loss in the trap amounted to only 1% of the probability of neutron β-decay. Another phenomenon studied in the experiment was the anomalous UCN loss during neutron storage in traps. Several explanations for these anomalous losses are given. The optimal coating of the trap walls for which no anomalous losses occur was found. The neutron lifetime obtained as a result of this experiment was $878.5 \pm 0.7_{stat} \pm 0.3_{sys}$ s. It differs by 5.6σ from the result of

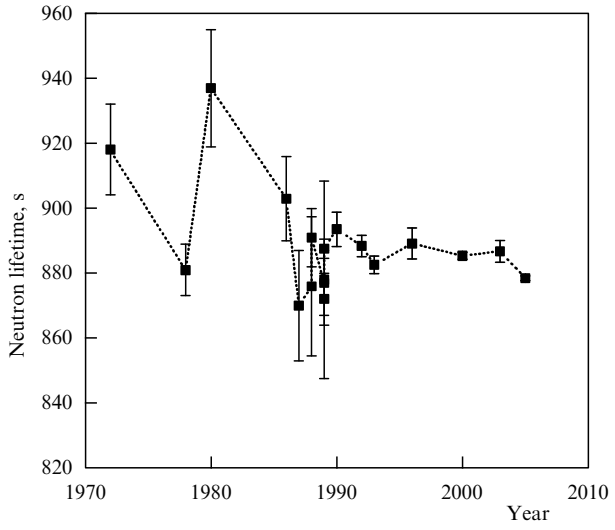

Figure 1. Progress in the accuracy of measuring the neutron lifetime.

Table 1. Results of experiments on measuring the neutron lifetime.

τ_n, s	Method	Author(s), year, reference
$878.5 \pm 0.7 \pm 0.3$	Storage	A P Serebrov et al. 2005 [20]
$886.8 \pm 1.2 \pm 3.2$	Beam	M S Dewey et al. 2003 [18]
$885.4 \pm 0.9 \pm 0.4$	Storage	S S Arzumanov et al. 2000 [9]
$889.2 \pm 3.0 \pm 3.8$	Beam	J Byrne et al. 1996 [21]
882.6 ± 2.7	Storage	W Mampe et al. 1993 [22]
$888.4 \pm 3.1 \pm 1.1$	Storage	V V Nesvizhevskii et al. 1992 [23]
$893.6 \pm 3.8 \pm 3.7$	Beam	J Byrne et al. 1990 [24]
887.6 ± 3.0	Storage	W Mampe et al. 1989 [25]
872 ± 8	Storage	A G Kharitonov et al. 1989 [26]
$878 \pm 27 \pm 14$	Beam	R Kossakowski et al. 1989 [27]
877 ± 10	Storage	W Paul et al. 1989 [28]
891 ± 9	Beam	P E Spivak et al. 1988 [29]
$876 \pm 10 \pm 19$	Beam	J Last et al. 1988 [30]
870 ± 17	Beam	M Arnold et al. 1987 [31]
903 ± 13	Storage	Yu Yu Kosvintsev et al. 1986 [32]
937 ± 18	Beam	J Byrne et al. 1980 [33]
881 ± 8	Beam	L N Bondarenko et al. 1978 [16]
918 ± 14	Beam	C J Christensen et al. 1972 [17]

Arzumanov et al. [9], and by 6.5σ from the world average value. At the end of the review we will analyze the possible reasons for such discrepancies. We will also discuss the effect of the new result for the neutron lifetime on the test of the unitary of the quark mixing matrix and on the analysis of the data in the nucleosynthesis model for the formation of the Universe.

3. Experimental facility for measuring the neutron lifetime with a gravitational UCN trap and the measurement methods

3.1 Experimental facility

The experimental facility was a joint project of the B P Konstantinov Petersburg Nuclear Physics Institute (PNPI), Gatchina and the Joint Institute for Nuclear Research (JINR), Dubna. It was first used together with the universal source of cold and ultracold neutrons from the water-moderated water-cooled reactor VVR-M in Gatchina (Russia). At first, the cooling of the facility to 10 – 15 K was done by a refrigerator. Later, the facility was modernized (a cryostat scheme was utilized) and became self-contained, which made it possible to perform measurements that involved using the high-flux ILL reactor in Grenoble (France). Figure 2 shows the modified version of the facility.

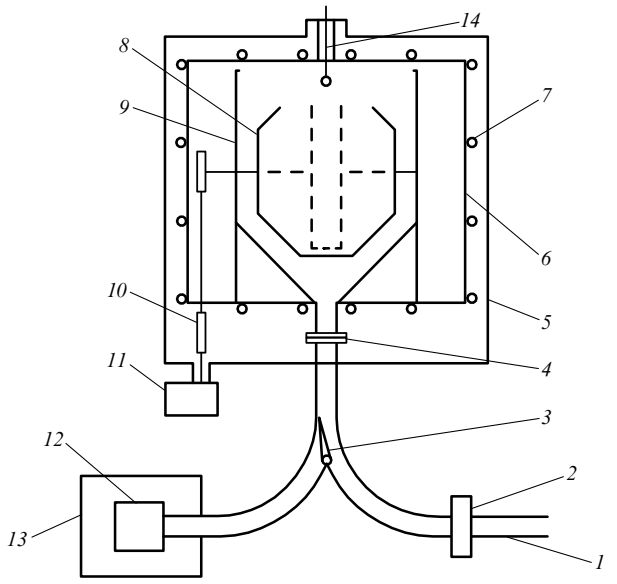

Figure 2. Schematic of the gravitational UCN storage system: *1*, input neutron guide for UCNs; *2*, inlet valve; *3*, selector valve (shown in the position in which the trap is being filled with neutrons); *4*, foil unit; *5*, vacuum volume; *6*, separate vacuum volume of the cryostat; *7*, cooling system for the thermal shields; *8*, UCN storage trap (the dashed lines depict a narrow cylindrical trap); *9*, cryostat; *10*, trap rotation drive; *11*, step motor; *12*, UCN detector; *13*, detector shield, and *14*, vaporizer.

The facility comprises a gravitational trap for UCNs, but it can also serve as a differential gravitational spectrometer. Hence, a distinctive feature of this experimental setup is the possibility of measuring the UCN energy spectrum after the neutron has been stored in the trap.

The UCN storage trap *8* is placed inside the vacuum volume of the cryostat *9*. The trap *8* has a window and can be rotated about the horizontal axis in such a way that the UCNs find themselves blocked by gravitational field in the trap when the window is in its uppermost position.

The ultracold neutrons enter the trap after traveling through the neutron guide *1*, the open inlet valve *2*, and the selector valve *3*. The filling of the trap by the ultracold gas occurs when the trap window is in the 'down' position. After filling the trap, it is rotated so that the window appears to be in the 'up' position.

The vacuum system has two separate vacuum volumes: the 'high-vacuum' (*6*), and the 'isolating' (*5*). The pressure in the high-vacuum volume of the cryostat amounts to 5×10^{-6} mbar. At such a pressure, the residual gas only slightly affects the storage time (0.4 s; see Section 6.4) of the UCNs in the trap. Heat exchange between the trap and the cryostat's reservoir was used in the cooling of the trap. To improve the heat exchange, gaseous helium was blown through the vacuum volume of the cryostat and later removed before measuring the neutron lifetime.

The position (height) of the trap window in relation to the bottom of the trap determines the maximum energy of the UCNs that can be retained in the trap. Different values of the window height correspond to different values of the cutoff energy in the UCN spectrum; in other words, a rotating trap

of this kind is a gravitational spectrometer. The spectral dependence of the neutron storage time can be measured through a series of rotations of the trap to the 'window-down' position. The trap was maintained in each intermediate position for 100 – 150 s to register the UCNs in the respective energy range. Using such a procedure, one can measure the spectrum of the trapped UCNs.

The neutron lifetime was measured by the size extrapolation method. To this end, two UCN traps with different dimensions were employed. The first trap was quasispherical and consisted of a cylinder 26-cm high and 84 cm in diameter that was 'crowned' by two truncated cones 22-cm high and 42 cm in diameter (the smaller diameter). The second trap was cylindrical, 14-cm high and 76 cm in diameter. The frequency of neutron collisions with the walls of the second trap was approximately 2.5 times higher than in the first trap. In Fig. 2, the narrow cylindrical trap is depicted by dashed lines.

A typical diagram of the counting rate at the detector in the measurement cycle is shown in Fig. 3. (This diagram, built on the basis of the results of the latest experiments at ILL, differs predominantly from the previous diagrams in that the detector counting rate is higher.)

At the beginning of a measurement cycle, the trap resides in the 'window-down' position, as it is being filled by UCNs. Then the trap is rotated into the monitoring position, in which the trap window height is approximately 10 cm lower than in the neutron storage position with its window 'up'. The filling process can be monitored by the UCN detector *12* (see Fig. 2) through a slit in the selector valve. After the trap has been rotated into the monitoring position, the selector valve is switched into the position in which UCNs are registered. The trap is maintained in the monitoring position for 300 s. During this period, neutrons with energies higher than the gravitational barrier leave the trap (see Fig. 3). Then the trap is rotated into the storage position. The procedure of neutron capture and preparation of the UCN spectrum takes about 700 s; in the left part of Fig. 3 the counting rate is presented on the log scale, while the counting rate for the subsequent procedures (700 – 3000 s) is presented with greater detail on the linear scale (the right part of Fig. 3). After a short (upper half of Fig. 3) or long (lower part of Fig. 3) storage time, the trap is rotated in step sequences through five positions, and in each of these positions it is kept motionless for 100 – 150 s, so the UCNs can be registered. The neutrons detected after each rotation have different mean energies. When all the UCNs have left the trap, the background count rate is measured. The angular positions of the trap window and the mean values of the UCN energies in each discharge are as follows:

$\theta = 30°$ (monitoring position);
$\theta = 40°$, $E_{\rm UCN} = 58$ cm;
$\theta = 50°$, $E_{\rm UCN} = 52$ cm;
$\theta = 60°$, $E_{\rm UCN} = 46$ cm;
$\theta = 75°$, $E_{\rm UCN} = 39$ cm;
$\theta = 180°$, $E_{\rm UCN} = 25$ cm.

The angles were chosen in such a way that there would be an equal number of UCNs for each segment of the UCN spectrum (unfortunately, the third portion was not successfully optimized, which is clearly obvious from Fig. 3).

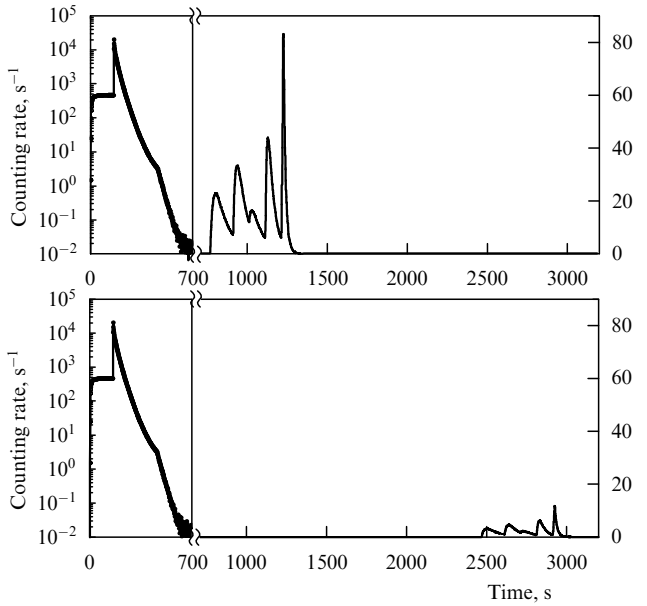

Figure 3. Time diagrams of the neutron storage cycle in a narrow trap for two different storage times.

3.2 Methods of extrapolation to the neutron lifetime. Basic relations

Any measurement of the neutron lifetime that follows the UCN storage method is based on the simple equation

$$\tau_{\rm st}^{-1} = \tau_{\rm n}^{-1} + \tau_{\rm loss}^{-1}\,. \tag{3.1}$$

Here, the total UCN loss probability $\tau_{\rm st}^{-1}$ comprises two terms, namely, the probability of neutron β-decay $\tau_{\rm n}^{-1}$, and the probability $\tau_{\rm loss}^{-1}$ of other possible UCN losses.

The UCN storage time $\tau_{\rm st}$ can be calculated if we know the measured number of neutrons that remain in the trap after two different storage times:

$$\tau_{\rm st} = \frac{t_2 - t_1}{\ln(N_1/N_2)}\,, \tag{3.2}$$

where N_1 and N_2 are the numbers of neutrons left in the trap after storage times t_1 and t_2, respectively. There is no need to know the efficiency of the UCN detector, the probability of UCN losses as the neutrons travel along the neutron guide, and so forth, since equation (3.2) uses only the ratio of the numbers of neutrons.

Since the UCNs are stored in a material trap, $\tau_{\rm loss}^{-1}$ contains the probability of loss at the trap walls:

$$\tau_{\rm loss}^{-1} = \mu\,(T, E)\,\nu(E)\,, \tag{3.3}$$

where $\mu(T, E)$ is the function of UCN losses due to reflection, which depends on the UCN energy and the temperature of the trap walls, and ν is the collision frequency of the UCNs with the trap walls, which depends on the UCN energy and the trap dimension. The function of UCN losses due to reflection, obtained on the assumption that the UCNs are reflected from a potential step with real (U_0) and imaginary (W) parts, can be represented in the following well-known form [34]

$$\mu(y) = \frac{2\eta}{y^2}\left(\sin^{-1} y - y\sqrt{1-y^2}\right)\begin{cases} \approx \pi\eta, & y \to 1 \\ \approx \dfrac{4}{3}\,\eta y, & y \ll 1\,, \end{cases} \tag{3.4}$$

where η is the loss factor determined by the ratio of the imaginary-to-real parts of the potential or the scattering amplitudes, $\eta = W/U_0 = b'/b$, and $y = (E/U_0)^{1/2}$.

In equation (3.4), the energy UCN loss function has been averaged over the incidence angles. Using the optical theorem, we can write down the imaginary part of the scattering amplitude in the following form [34]

$$b' = \frac{\sigma_{\rm abs} + \sigma_{\rm upscat}(T)}{2\lambda} .$$

The capture and inelastic-scattering cross sections are proportional to the neutron wavelength λ, with the result that neither b' nor η depend on λ or the neutron energy E. However, the loss factor is temperature-dependent, $\eta = \eta(T)$, due to the temperature dependence of the inelastic-scattering cross section $\sigma_{\rm upscat}(T)$.

Now we can rewrite the right-hand side of equation (3.3) as the product of two factors: one depending only on the UCN energy, and the other only on the trap temperature:

$$\tau_{\rm loss}^{-1} = \eta(T)\,\gamma(E)\,, \tag{3.5}$$

where $\eta(T)$ is the UCN energy-independent loss factor, and $\gamma(E)$ is the effective collision frequency which depends on the UCN energy and the trap dimensions. The neutron lifetime can be obtained via linear extrapolation of $\tau_{\rm st}^{-1}$ to the zero value of γ. The UCN loss factor η proves to be equal to the tangent of the slope angle of the extrapolation line. Different values of the effective UCN collision frequency γ can be obtained by using traps of different dimensions and/or different values of the UCN energy. The effective frequency γ of UCN collisions with the trap walls can be computed.

3.3 The energy extrapolation method

To calculate the energy dependence of losses $\tau_{\rm loss}^{-1}$ that allows for UCN motion in a gravitational field, a numerical integration method and the Monte Carlo method were employed. The loss probability was evaluated by the simple formula $\tau_{\rm loss}^{-1} = \mu(E)\,\nu(E)$. The UCN collision frequency $\nu(E)$ is equal to the UCN flux directed onto a surface area $\mathrm{d}S$, namely, $(1/4)\,v\rho(v)\,\mathrm{d}S$, where $\rho(v)$ is the UCN number density which depends on the UCN velocity v. In a gravitational field, the UCN number density is proportional to $\sqrt{(E-mgh)/E}$, where E is the UCN energy at the base of the trap, and h is the height measured from the base of the trap. Since the UCN kinetic energy depends on h, the above formula must be integrated with respect to h and then normalized:

$$\tau_{\rm loss}^{-1}(E) = \frac{\int_0^E \mu(E-h')\,v(E-h')\,\rho(E-h')\,\mathrm{d}S(h)}{4\int_0^E \rho(E-h')\,\mathrm{d}V(h)} , \tag{3.6}$$

where $h' = mgh$.

To compare the results produced by this formula with the experimental data, we must integrate it over the energy interval of each measurement and allow for the real spectral distribution of the UCN number density in the trap. The UCN spectrum in the trap was measured immediately after completion of the monitoring process by the procedure reproduced in the upper part of Fig. 3. We also allowed for modifications of the spectrum during UCN storage in the trap, the factor of which provides a small correction to the computed function γ ($\Delta\gamma/\gamma = 0.1\%$, or 0.01 s for the extrapolated neutron lifetime). Additional corrections to the computed function γ were also made, so as to take into account the incomplete discharge of UCNs for each energy interval, as Fig. 3 implies. This may produce a correction up to 0.7 s in the extrapolated neutron lifetime. However, using the results of detailed numerical simulations by the Monte Carlo method and the size extrapolation method (see Section 3.4), we can reduce this correction and obtain an uncertainty in the extrapolation to the neutron lifetime amounting to about 0.24 s.

Using the calculated values of the loss factor for different energies, $\tau_{\rm loss}^{-1} = \eta(T)\,\gamma(E)$, we can extrapolate the measurement data and find the neutron lifetime. The result of such an extrapolation depends on the function $\mu(E)$ which actually may differ somewhat from that of the adopted form (3.4), for example, it can be specified by a certain function $\mu'(E)$. To reduce the systematic effect caused by the uncertainty in the energy dependence $\mu'(E)$, we must examine the possibility of excluding the effect of the energy dependence of the loss factor on the extrapolation results.

3.4 The size extrapolation method

To exclude the effect of the energy dependence $\mu'(E)$ on the result, we can make extrapolation to zero losses by using data on the storage of UCNs with the same mean energy in traps of different dimensions. Using relationships (3.1) and (3.5) for two traps with storage times τ_1 and τ_2, namely

$$\tau_1^{-1}(E) = \tau_{\rm n}^{-1} + \eta\gamma_1(E)\,, \tag{3.7}$$

$$\tau_2^{-1}(E) = \tau_{\rm n}^{-1} + \eta\gamma_2(E)\,, \tag{3.8}$$

we find that

$$\tau_{\rm n}^{-1} = \tau_1^{-1}(E) - \frac{\tau_2^{-1}(E) - \tau_1^{-1}(E)}{\gamma_2(E)/\gamma_1(E) - 1} . \tag{3.9}$$

Thus, the effect of the energy dependence $\mu'(E)$ is excluded almost entirely because the final result for the neutron lifetime depends only on the ratio $\gamma_2(E)/\gamma_1(E)$. Clearly, in the absence of gravitation, by employing equations (3.7) and (3.8) for two different traps and a certain energy we can totally exclude the function $\mu'(E)$. In reality, where there is gravitation, complete exclusion of $\mu'(E)$ is impossible because of the integral equation (3.6). However, the residual effect of the dependence $\mu'(E)$ on the neutron lifetime was negligible. For instance, in our last experiment the contribution from this dependence amounted to 0.14 s, while the statistical accuracy of the measurements was 0.7 s.

The size extrapolation method based on the idea of using two traps makes it possible to substantially reduce systematic errors which are caused by the uncertainty of our knowledge about the function $\mu'(E)$.

4. The first experiments on measuring the neutron lifetime with gravitational UCN traps

4.1 Measurement of $\tau_{\rm n}$ in a trap with a beryllium coating and revealing the anomalous loss problem

In the first experiments involving a gravitational trap, the trap walls were coated with beryllium. This choice was determined by the fact that beryllium possesses a small neutron-capture cross section and a high Debye temperature, with the result that the inelastic-scattering cross section rapidly enough falls off with decreasing temperature. Already at liquid-nitrogen temperatures, the inelastic-scattering cross section drops to the value of the neutron-capture cross section by beryllium.

Although earlier experiments (see Ref. [35]) showed that the interaction cross section for UCNs during storage in traps with beryllium coatings is much higher than the calculated value, we believed that this problem could be resolved. An alternative solution, i.e., using solid oxygen as the coating material, was also considered. In the preparation stages of the experiment, the dominant opinion was that anomalous losses are caused by the presence of hydrogen on the surface, and we planned to remove the hydrogen by heating the trap walls in a vacuum, by using deuterium as a substitute for hydrogen, and by operating in the low-temperature range, $\sim 10-15$ K. Indeed, the heating and isotope substitution procedures made it possible to reduce the loss factor considerably; nevertheless, we found that there was an unremovable contribution to the loss factor at a level of 3×10^{-5} per collision.

Figure 4 depicts the temperature dependences of the UCN loss factor for neutrons stored in beryllium traps [36]. We see that the UCN loss factor depends on the hydrogen concentration at the trap surface and on the trap's temperature. At low temperatures, where the process of UCN inelastic scattering is almost completely suppressed, the UCN loss factor is, nevertheless, equal to 3×10^{-5} and exceeds the expected value by a factor of about ten. It is this excess factor that is called the anomalous loss in beryllium.

What is most remarkable in this effect is that after removing all traces of hydrogen the anomalous UCN loss becomes temperature-independent (the difference in the respective data points for curves *4* and *5* in Fig. 4 remains practically the same). At the same time, the results of the experiments conducted by Arzumanov et al. [37] and Varlamov et al. [38] show that the lost neutrons appear outside the trap as inelastically scattered.

In view of the large magnitude of the loss factor for a beryllium coating, it was decided to investigate the case of a solid-oxygen coating and, for the time being, to leave the study of the problem of anomalous losses for the future.

The use of solid-oxygen coatings at a trap temperature of about 10 K made it possible to reduce the loss factor to 6×10^{-6} per collision. This in itself is a considerable step forward, which allows us to measure the neutron lifetime with a gravitational UCN trap.

4.2 Measurement of τ_n in a trap with a solid-oxygen wall coating

The first measurements of τ_n with a trap coated by solid oxygen were carried out using an aluminium quasispherical trap. Extrapolation to the neutron lifetime was done by studying the energy dependence of losses. The first result for the neutron lifetime was 872 ± 8 s [25], but the accuracy of these measurements proved to be low due to the insufficient base of extrapolation along the axis of the effective collision frequency γ. Hence, the experiment was augmented by measurements involving a flat cylindrical trap.

The results of these experiments are given in Fig. 5, which is a graphic illustration of equations (3.7) and (3.8). In it, the experimental values of τ_{st}^{-1} (vertical axis) are plotted against the calculated argument γ (horizontal axis). Measurements involving beryllium traps, which produced results with lower statistical accuracy, were done to demonstrate the conditions of measurements prior to oxygen sputtering.

The established experimental values of the neutron lifetime were as follows: $\tau_n = 885.0 \pm 7.7$ s for traps with a beryllium coating, and $\tau_n = 889.0 \pm 3.1$ s for traps with an oxygen coating. The loss factor η was $(28.1 \pm 4.0) \times 10^{-6}$ for beryllium, and $(6.1 \pm 0.6) \times 10^{-6}$ for oxygen. The value of the normalized quantity χ^2, which corroborates the validity of the extrapolation made, amounted to 0.81 for traps with an oxygen coating. The final result for the neutron lifetime, obtained in the given experiment, was 888.4 ± 3.3 s [23].

This result was obtained at the water-moderated water-cooled reactor VVR-M in Gatchina, where the UCN number density is five times lower than that at the high-flux ILL reactor in Grenoble (France). Hence, one of the prospects of increasing the measurement accuracy was related to the possibility of conducting an experiment at the ILL reactor. However, the problem of anomalous losses, which vividly manifested itself in the case with beryllium, still remained unresolved. This situation was a source of anxiety about the validity of the energy extrapolation method, since the energy

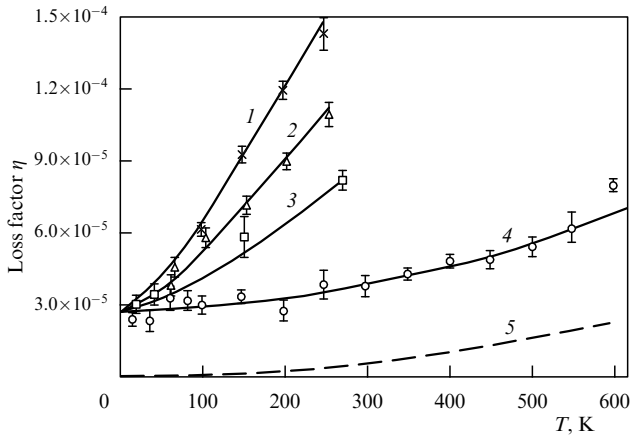

Figure 4. Temperature dependence of the UCN loss factor η for different beryllium traps: *1*, beryllium-sputtered spherical trap without degassing; *2*, degassed (5 hours at 250 °C) beryllium-sputtered cylindrical trap; *3*, degassed (8 hours at 300 °C) all-metal beryllium trap; *4*, degassed (28 hours at 350 °C with a flow of He and D_2) beryllium-sputtered spherical trap, and *5*, theoretical temperature dependence calculated within the Debye model.

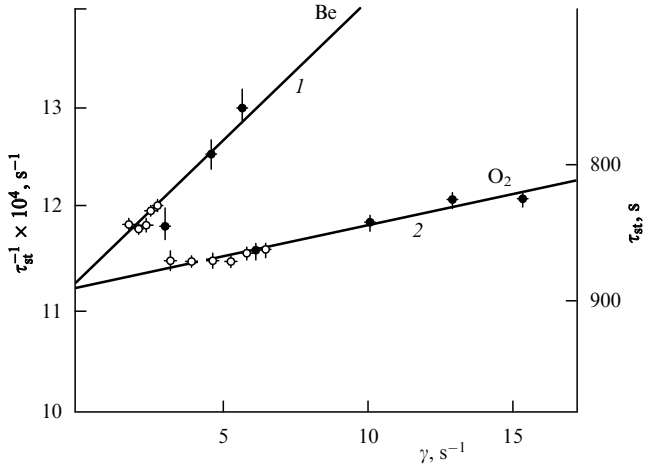

Figure 5. Results of measuring τ_{st}^{-1} as a function of the calculated parameter γ: *1*, extrapolation to the value of the neutron lifetime according to the data for traps with beryllium coatings; *2*, extrapolation to the value of the neutron lifetime according to the data for traps with an oxygen coating and a beryllium sublayer; ○, measurement results for a spherical trap, and •, measurement results for a cylindrical trap.

dependence of the anomalous loss could differ from the classical dependence (3.4) derived from neutron-optical calculations. It was still unclear to what extent the losses in solid oxygen are anomalous, since the inelastic-scattering cross section by solid oxygen had not been measured.

The next stage in our research was devoted mainly to the nature of anomalous losses. Since these losses manifest themselves most clearly in beryllium, this element was chosen as the main object of our investigations.

5. The problem of anomalous UCN losses during storage in material traps and its solution

5.1 General description of the problem

Even the first experiments on UCN storage in material traps [39, 40] showed that UCN losses under reflection are much higher than the results predicted by calculations done on the basis of neutron optics for a perfect surface. Subsequent experiments revealed that there is UCN heating on hydrogenous impurities present on the surface [41, 42]. However, to explain the loss factor of about 10^{-3}, the concentration of hydrogen at the surface must be exceptionally high (e.g., the concentration must correspond to a layer of water or oil approximately 100 Å thick). By using poorly absorbing materials and cooling the trap to low temperatures, the loss factor η was reduced to $(2-3)\times 10^{-5}$ and even 2×10^{-6}. Table 2 lists the results of measurements of the loss factor η for the hydrogen-free Fomblin oil at room temperature, beryllium, solid oxygen, graphite, and low-temperature (LT) Fomblin in the solid state.

Table 2. Some of the best values of UCN loss factors for different materials.

Material	Loss factor η	References
Fomblin (300 K)	$(2.2\pm 0.1)\times 10^{-5}$	[43]
Be (6.5 K)	3.2×10^{-5}	[44]
Be (10 K)	$(2.8\pm 0.4)\times 10^{-5}$	[23]
O_2 (10 K)	$(6.1\pm 0.6)\times 10^{-6}$	[23]
Graphite (100 K)	$(5.0\pm 0.5)\times 10^{-5}$	[37]
LT Fomblin (110 K)	$(2.2\pm 0.2)\times 10^{-6}$	[20]

Among these results, the discrepancy between the expected and experimental values is especially evident for beryllium and graphite. The interaction cross section for neutrons moving in matter with a velocity of $10-12$ m s^{-1} was measured for beryllium. Basing our reasoning on the results of measurements of the interaction cross section inside matter, we could expect the UCN loss factor due to reflection to be smaller than 2×10^{-6}. However, the experiment demonstrated that for beryllium at $6-10$ K the loss factor is on the order of 3×10^{-5} [34, 35].

A similar situation takes place for graphite, with the loss factor being equal to 5×10^{-5} when UCNs at 80 K are reflected by the graphite surface. And again, this value of the loss factor exceeds estimates obtained from experimental inelastic-scattering and capture cross sections for cold neutrons by a factor greater than ten.

For solid oxygen, the calculated loss factor is smaller than the experimental value by a factor of ten. However, since there are no experimental data on the inelastic-scattering cross section for neutrons with low energies at low temperatures, we can draw no final conclusion in the case of solid oxygen.

For Fomblin oil, no discrepancies between the calculated values and the experimental results were found. At room temperature, quasielastic scattering by surface waves was detected. This fact can explain the value $10^{-5}-10^{-6}$ for the experimental loss factor [45, 46]. The process is suppressed upon solidification of Fomblin [46, 47]. For LT Fomblin at 110 K, at which it is solid, the value $(2.2\pm 0.2)\times 10^{-6}$ [20] of the measured loss factor does not contradict the results of measurements of the inelastic-scattering cross section [48].

Thus, there are at least two experimentally proven examples of anomalous UCN losses in materials in which the cross section of UCN interaction upon subbarrier reflection is much larger than the cross section at energies exceeding the barrier (the cases of beryllium and graphite). At the same time, there is an experimental example in which the subbarrier and over-barrier reflection cross sections are roughly the same, and this refers to LT Fomblin oil at 110 K.

It is for this reason that LT Fomblin at 110 K was selected as the coating material for the next experiment with a gravitational UCN trap.

However, let us once more turn to the problem of anomalous UCN losses and examine a number of experimental studies in this area of research and the proposed solution of the problem.

The main paradox in the anomalous-loss problem is the fact that the cross section of this additional process is temperature-independent, although the larger fraction of the lost UCNs prove to be inelastically scattered [37, 38]. It is very difficult to imagine a temperature-independent process of neutron inelastic scattering.

There have been various attempts to explain the anomalous UCN losses under reflection. However, in these attempts the researchers either give no explanation of the temperature independence of such losses, especially in the low-temperature region [37, 49], or discuss effects whose probability is much lower than that of anomalous losses [50].

We proposed an entirely new mechanism of UCN losses [51–53]. This mechanism is based on the fact that the cross section of the UCN interaction with defects (~ 100 Å) of polycrystalline materials is much greater under the subbarrier reflection of UCNs than in over-barrier transmission of cold neutrons. This mechanism provides an explanation for the temperature independence of the effect, despite the fact that the process is primarily inelastic.

The main idea of our research was that the UCN reflection process is not entirely coherent; rather, it is accompanied by an additional incoherent process of scattering when the UCNs interact with the surface of the substance.

The incoherent process under UCN reflection could be confirmed by the discovery of UCN depolarization during neutron storage.

5.2 UCN depolarization during neutron storage in beryllium traps and the possible link between depolarization and anomalous UCN losses under reflection

An experiment on measuring UCN depolarization during neutron storage in traps could serve as a test of incoherent UCN scattering under reflection from matter. Such experiments have been carried out and UCN depolarization was discovered when the neutrons were stored in beryllium traps [54, 55]. If we assume that after the incoherent process the neutrons are scattered by an angle of 4π, then only half the incoherently scattered neutrons return to vacuum (to the trap), and only two-thirds of this half have flipped their

spin. The temperature independence of the depolarization process, measured in this experiment (see Ref. [55]), suggests that the UCNs that were incoherently scattered in matter do not return to vacuum. In this way, an incoherent process was detected.

The spin-flip probability normalized to one collision amounted to $(1-2)\times 10^{-5}$. It should be emphasized that the probability of UCN spin flip proved to be close to the probability of anomalous losses.

Thus, there are certain indications that depolarization is linked to the occurrence of anomalous losses due to incoherent scattering by beryllium defects.

The defect structure of the beryllium polycrystalline structure was studied by letting UCNs pass through beryllium samples and coatings.

5.3 Studying the passage of UCNs through beryllium samples and beryllium coatings

The results of studying the passage of neutrons with a velocity of $10-12$ m s^{-1} through beryllium samples are shown in Fig. 6, which depicts the temperature dependences of the macroscopic cross section for the interaction of very cold neutrons in their passage through different beryllium samples: pressed, quasi-single-crystal, and melted.

Figure 6 clearly demonstrates that at low temperatures, when the UCN inelastic-scattering cross section is suppressed, the macroscopic cross section of elastic scattering by the defects of the material amounts to $1-2$ cm^{-1}. Notice that allowing for this cross section in calculations in the neutron-optics model cannot explain the anomalous UCN loss in the case of beryllium.

The passage of UCNs through beryllium coatings sputtered on aluminium (15 μm) and copper (10 μm) foils and on silicon plates (350 μm) was studied at the ILL reactor using the PNPI gravitational spectrometer. The goal of these studies reduced to examining the quality of sputtered coatings. Moreover, the following question was posed: if there are anomalous UCN losses under neutron reflection, can the anomalous passage of UCNs through a thin coating be observed?

A similar experiment had already been carried out before (see Ref. [56]), and excess passage of UCNs through beryllium coatings was discovered. However, it remained unclear whether this occurred due to the quality of the coatings or whether the passage through thin coatings was due to an incoherent process.

In the new experiment, 15 different samples were investigated, and the passage of the UCNs whose energies exceeded the limiting energy of the substrate but were lower than the limiting energy of beryllium was observed (Fig. 7). The penetration probability through $(2-6)\times 10^3$-Å thick beryllium coatings deposited on aluminium and copper foils was found to vary from 2×10^{-5} to 1×10^{-4}, with the mean value being 4×10^{-5}. Some foils were coated twice on the same side. After the first sputtering, they were flushed out with alcohol in order to clean the areas covered earlier by dust particles and to be able to cover the defect regions in the second sputtering. However, this did not help to reduce the transmission of UCNs. The foils sputtered on both sides did not let the UCNs through. Only the upper limit on transmittance equal to 1×10^{-6} was established for such foils.

Thus, it was found that the fraction of the defect surface for beryllium coatings on aluminium and copper foils amounts to 4×10^{-5} on the average. However, for experiments on storing UCNs with energies lower than the critical energy for aluminium or copper, such a defect structure of the

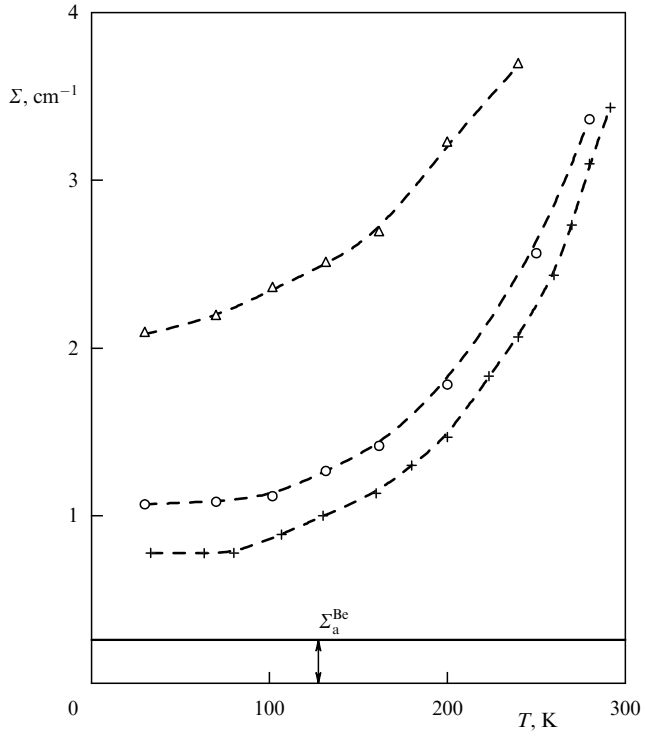

Figure 6. Temperature dependence of the macroscopic cross section Σ for beryllium: △, pressed; ○, quasi-single-crystal, and +, melted. $\Sigma_a^{Be}=\rho^{Be}\sigma_a^{Be}$ is the macroscopic capture cross section by beryllium nuclei.

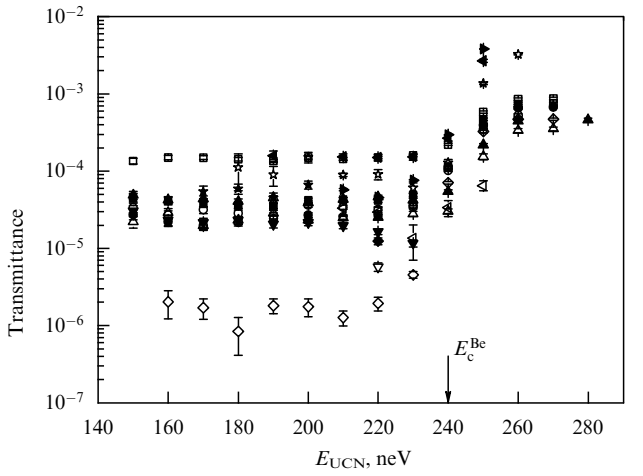

Figure 7. Dependence of transmittance on the UCN energy. Passage through beryllium-sputtered foils: ■, Al (20 μm) + Be (2150 Å) + Be (2150 Å)*; □, Al (20 μm) + Be (2150 Å) + Be (2150 Å); •, Al (15 μm) + Be (2150 Å) + Be (2150 Å)*; ○, Al (20 μm) + Be (2150 Å) + Be (2150 Å)*; ▲, Al (15 μm) + Be (3500 Å); △, Al (15 μm) + Be (6100 Å); ▼, Si-plate (300 μm) + Be (2150 Å); ▽, Si-plate (300 μm) + Be (2150 Å); ◆, Si-plate (300 μm) + Be (2150 Å) + Be (2150 Å)*; ◇, Si-plate (300 μm) + Be (2150 Å) + Be (2150 Å)*; ★, Si-plate (300 μm) + Be (2150 Å); ☆, Cu (10 μm) + Be (6100 Å); ◁, Cu (10 μm) + Be (3500 Å); ◀, Cu (10 μm) + Be (3500 Å), and ▶, Cu (10 μm) + Be (3500 Å). The asterisk* indicates that there was double sputtering from one side with the surface cleaned with alcohol after the first sputtering, and E_c^{Be} stands for the beryllium critical energy under UCN reflection.

surface cannot play an important role, since the neutrons would be reflected from the substrate. For the defect structure of the surface to justify neutron losses of about $(2-3)\times 10^{-5}$, we must assume that after being scattered by a defect a substantial fraction of UCNs is absorbed in matter. For instance, an explanation for the anomalous UCN losses under reflection can be explained if we assume that after incoherent scattering by a defect the neutrons scattered in a medium do not return to the trap (vacuum).

5.4 Measuring the energy dependence of anomalous UCN losses in beryllium

A detailed study of the energy dependence of anomalous UCN losses in beryllium was done at the ILL reactor, where thanks to the high UCN number density and prolonged measurements we were able to discover that the energy dependence of the losses does not agree with the calculated one if one remains within the framework of coherent reflection, i.e., equation (3.4).

Figure 8 portrays the energy dependence of UCN losses, $\tau_{\rm loss}^{-1}$, during neutron storage in a narrow cylindrical trap for which the contribution of losses is greater and the energy dependence can be revealed with a higher accuracy than for a spherical trap.

It should be noted that because of the presence of a gravitational field, the relationship between $\tau_{\rm loss}^{-1}(E)$ and $\mu(E)$ cannot be a directly proportional one, but still it can easily be calculated. The solid heavy curve represents the calculated dependence for beryllium, where $\mu(E)$ was chosen with a free parameter. This parameter was chosen to fit the calculated and the experimental values at the first point in energy.

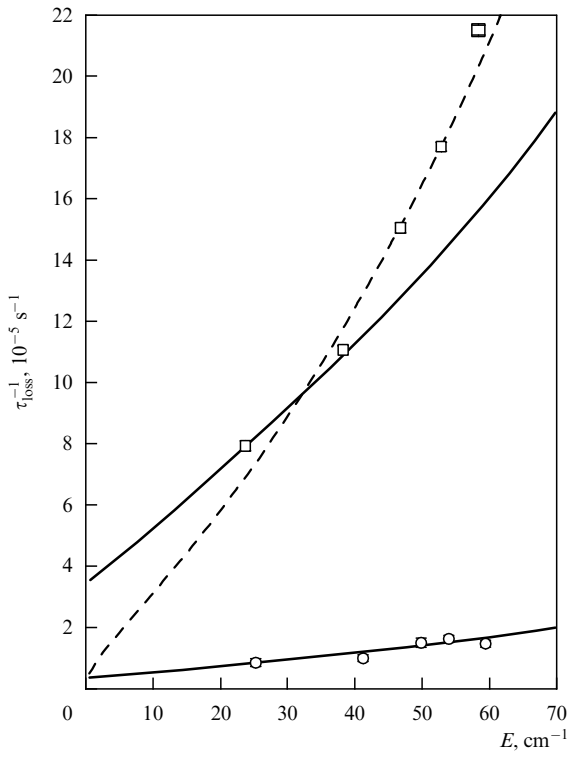

Figure 8. Energy dependence of the probability of UCN losses during neutron storage in a narrow cylindrical trap. To calculate the loss, the neutron lifetime was taken from the experiment involving a trap with an LT Fomblin coating at 110 K: □, beryllium trap at 90 K, and ○, trap with an LT Fomblin coating at 110 K.

Figure 8 demonstrates that the experimental and calculated dependences do not agree. Hence, the UCN loss factor for beryllium can be described by the neutron-optics model neither in magnitude nor in the character of the dependence. At the same time, for LT Fomblin oil at 100 K, the behavior of the experimental energy dependence does not contradict that of the calculated one.

Thus, we have found a coating (LT Fomblin oil at a temperature $T = 110$ K) for which there are no anomalous UCN losses.

5.5 Explaining the phenomenon of anomalous UCN losses via the effect of UCN capture by defects in matter

The problem of anomalous UCN losses in the course of neutron storage in traps led to the idea that it is possible to localize UCNs in a medium [51]. In this section, we will attempt to find a simple theoretical description of the UCN scattering and capture by defects in a medium. But first let us recall the ordinary neutron-optical representation [34, 57, 58].

The coherent UCN – substance interaction is specified by a potential with real and imaginary parts:

$$V(\mathbf{r}) \approx U - \mathrm{i}W, \quad U = \frac{2\pi\hbar^2}{m}\,\rho\,\mathrm{Re}\,b\,, \quad W = \frac{2\pi\hbar^2}{m}\,\rho\,\mathrm{Im}\,b\,,$$

where ρ is the nucleus number density per unit volume. The imaginary part of the potential describes neutron capture and inelastic scattering. The typical values of the potential are $U \approx 10^{-7}$ eV and $|W/U| \approx 10^{-4}$.

When $E_0 > U$, an ordinary plane wave $\exp(\mathrm{i}kz)$ propagates in a medium with a wave vector

$$k = \frac{1}{\hbar}\sqrt{2m(E_0 - U + \mathrm{i}W)} \equiv k' + \mathrm{i}k''\,,$$

$$k' \approx \frac{1}{\hbar}\sqrt{2m(E_0 - U)}\,, \quad k'' \approx \frac{W}{2\hbar}\sqrt{\frac{2m}{E_0 - U}}\,.$$

The damping of the wave in a medium is determined by the imaginary part of the potential.

When $E_0 < U$, a damped wave $\exp(-\varkappa z)$ propagates in a medium with a wave vector

$$\varkappa = \frac{1}{\hbar}\sqrt{2m(U - E_0 - \mathrm{i}W)} \equiv \varkappa' - \mathrm{i}\varkappa''\,,$$

$$\varkappa' \approx \frac{1}{\hbar}\sqrt{2m(U - E_0)}\,, \quad \varkappa'' \approx \frac{W}{2\hbar}\sqrt{\frac{2m}{U - E_0}}\,.$$

A traveling wave in a medium is determined by the wave vector $\varkappa''$, or the imaginary part of the potential.

The coefficient of coherent UCN reflection from particles in a medium for normal incidence with a UCN energy E_0 is given by the formula

$$R = \left|\frac{k_0 - k}{k_0 + k}\right|^2, \tag{5.1}$$

where $k_0 = \sqrt{2mE_0}/\hbar$, and $k = \sqrt{2m(E_0 - U + \mathrm{i}W)}/\hbar$.

This yields the following expression for the loss factor in coherent UCN reflection with $E_0 < U$:

$$\mu = 1 - R = 2\eta\sqrt{\frac{E_0}{U - E_0}}, \tag{5.2}$$

where $\eta = \mathrm{Im}\,b/\mathrm{Re}\,b$.

Using the optical theorem $\sigma_{\rm tot} = 4\pi\,{\rm Im}\,b/k_0$, we can reduce formula (5.2) to the following one

$$\mu = 2\sigma_{\rm tot}\rho\hat{\lambda}\,\frac{E_0}{U}\,, \tag{5.3}$$

where $\hat{\lambda} = \hbar/\sqrt{2m(U-E_0)}$ is the penetration depth of UCNs to the medium interior, and E_0/U is the amplitude of the probability density at the surface of the medium. Of course, the cross sections of neutron inelastic scattering and capture play a decisive role in determining the value of $\sigma_{\rm tot}$.

Equation (5.3) can be interpreted as the attenuation of the UCN flux in its passage through the surface layer of substance of thickness $2\hat{\lambda}$.

Now let us examine the influence of defects on the process of UCN reflection by employing the approach proposed in Refs [51, 52].

The substance density may rapidly decrease near a defect, with the result that incoherent scattering is possible from the defect. The presence of hydrogen (in the form of H_2O or H_2) in an intercrystalline defect may also be the reason for incoherent scattering with depolarization. The most interesting case is coming into play when $E_0 < U$.

The Schrödinger equation for a homogeneous medium with a material defect has the form

$$\left(\frac{\hbar^2}{2m}\,\nabla^2 + E_0\right)\psi(r) = \left(U - {\rm i}W + \frac{2\pi\hbar^2 B}{m}\,\delta(r)\right)\psi(r). \tag{5.4}$$

Here, $B = nb$ is the scattering length from a defect, which is equal to the nucleus scattering length multiplied by the number of nuclei. The scattering amplitude F is simply equal to $-B$. We examine the simplest case where the defect size (100 Å) is much smaller than the neutron wavelength (1000 Å). Hence, we will describe the defect by a delta function and use the s-wave approximation.

Detailed study of this problem was presented in Ref. [53]. Here, we only give the final result for the total scattering cross section by a defect for the opposite cases $E_0 > U$ and $E_0 < U$.

Equation (5.4) can be solved by employing perturbation-theory techniques, i.e., we first solve the equation with the potential $U - {\rm i}W$ and arrive at solutions mentioned above for $E_0 > U$ and $E_0 < U$. Then we examine the scattering by a defect described in the case at hand by a delta function and calculate the cross sections of scattering and capture by the defect for $E_0 > U$ and $E_0 < U$.

For the total cross section in the case $E_0 > U$, we obtain the fairly obvious result

$$\sigma_{\rm tot}|_{E_0>U} = 4\pi\,\frac{{\rm Im}\,F}{k'}\,, \tag{5.5}$$

which is an analog of the optical theorem for the medium.

Similarly, for scattering by a defect with $E_0 < U$ we have

$$\sigma_{\rm tot}|_{E_0<U} = \frac{4\pi\,{\rm Im}\,F}{\varkappa''}\,, \tag{5.6}$$

but the denominator contains the wave vector in the medium, which is proportional to the imaginary part of the medium's potential.

Notice that $k'/\varkappa'' \approx (E_0 - U)/W \approx 10^4$, with the result that the cross section of neutron interaction with the defect is much larger when $E_0 < U$ than when $E_0 > U$.

This effect of enhancement of the neutron-capture cross section by a defect emerges because of localization of UCNs with an energy $E_0 < U$ around the material defect. It is related to the fact that scattering at negative energies, which is possible only in the surface layer, takes place with the wave vector $\varkappa''$.

Another important advantage of the model proposed is that it explains the paradox of the temperature independence of anomalous neutron losses. When the material defects contain no other elements, both ${\rm Im}\,F$ and $\varkappa''$ are proportional to ${\rm Im}\,b = (\sigma_{\rm inel}(T) + \sigma_{\rm abs} + \sigma_{\rm incoh.\,scat})\,k/4\pi$. Thus, ${\rm Im}\,b$ in the numerator and denominator of formula (5.6) cancel out. The temperature dependence effect disappears, although the interaction process may be inelastic. This explains the main paradox of anomalous losses.

The probability of anomalous losses can be estimated by a formula similar to Eqn (5.3), since the latter properly takes into account the distribution of the probability density of finding a neutron in the surface layer. However, one should now use the cross section of neutron interaction with a defect, $\sigma_{\rm tot.\,def}$, and the defect number density $N_{\rm def}$:

$$\mu_{\rm a} = 2N_{\rm def}\,\sigma_{\rm tot.\,def}\,\hat{\lambda}\frac{E_0}{U}\,. \tag{5.7}$$

Let us assume that the linear dimension of a typical defect is $L = 100$ Å, the typical volume that such a defect occupies is 100^3 Å^3, and the substance density inside the defect comprises 50%.

The defect number density for beryllium can be calculated by using the experimental data on the passage of cold neutrons through beryllium samples (see Fig. 6). The macroscopic cross section of the interaction of very cold neutrons with beryllium at $T = 30$ K is determined by the cross section of scattering by defects and amounts to $1-2$ cm^{-1}. The scattering cross section by a defect containing n atoms $(n = 0.5\rho(100\ \text{Å})^3 = 0.6\times 10^5)$ with a scattering length $b = 0.8\times 10^{-12}$ cm is given by the following formula

$$\sigma_{\rm scatt.\,def} = 4\pi(nb)^2 = 2.9\times 10^{-14}\ {\rm cm}^2\,. \tag{5.8}$$

This formula yields the following estimate for the defect number density: $N_{\rm def} = (3.5-7)\times 10^{13}$ cm^{-3}.

Using the expressions for $\varkappa''$ and W, we can represent the total cross section of the neutron interaction with a defect for $E_0 < U$ as follows:

$$\sigma_{\rm tot.\,def} = \frac{4\pi\,{\rm Im}(nb)}{\varkappa''} = \frac{2n}{\hat{\lambda}\rho} = 0.8\times 10^{-12}\ {\rm cm}^2\,. \tag{5.9}$$

The formula for the anomalous loss probability then becomes

$$\mu_{\rm a} = 4\,\frac{N_{\rm def}}{\rho}\,n\,\frac{E_0}{U} \approx (2-3)\times 10^{-5}\,. \tag{5.10}$$

Of course, in the model adopted it is assumed that all atoms of a defect, in contrast to the atoms of the medium, scatter the neutrons incoherently. This condition is met if the defect contains hydrogen atoms. The presence of hydrogen in the substance defects is highly probable. Notice that the problem of neutron scattering from pores was examined in Ignatovich's book [34, pp. 132 and 165], but without allowance for incoherent scattering inside the pores. Without examining the incoherent process (basically caused by the presence of hydrogen in the pores) it is impossible to obtain a substantial increase in UCN losses resulting from reflection.

Thus, equation (5.10) produces a result according to which the anomalous neutron losses are proportional to the

ratio of the number of incoherently scattering atoms to the total number of atoms, i.e., n/ρ, which is quite obvious. The above estimate of the anomalous losses for beryllium is very close to the experimental result, but it must be noted that the parameter n (the size of the defect and the atomic number density inside the defect) was chosen arbitrarily. Nevertheless, the model proposed successfully explains the reason for anomalous UCN losses when the neutrons are reflected from beryllium nuclei and even indicates that the typical size of a defect that is the cause of incoherent scattering must be on the order of 100 Å. It turns out that a defect causing incoherent neutron scattering has a size roughly equal to the penetration depth $\hat{\lambda}$ of UCNs to a medium. Indeed, formula (5.9) shows that the total cross section of UCN–defect interaction, $\sigma_{\text{tot. def}}$, is proportional to n, or L^3. Hence, $\sigma_{\text{tot. def}}$ increases very rapidly with the defect size as long as $L < \hat{\lambda}$ and becomes equal to the cross-sectional area of the defect when $L \geqslant \hat{\lambda}$.

It is believed that the anomalous loss effect is a general one and manifests itself in all substances with hydrogen-containing defects. For instance, the macroscopic elastic-scattering cross section, which serves as indication of the presence of defects in the substance, for aluminium and zirconium foils amounts to 10–20 cm^{-1}. With these magnitudes of the macroscopic cross section one should expect an even higher value of the defect number density than in beryllium, and the level of anomalous losses may be as high as $(3-6) \times 10^{-4}$.

Note that the presence of hydrogen (in the form of H_2O or H_2) inside the defects substantially increases the anomalous UCN loss and leads to enhanced inelastic scattering and UCN capture by hydrogen. The formula used for estimating the anomalous loss that allows for the presence of hydrogen becomes

$$\mu_{\text{a}} = \frac{N_{\text{def}}}{\rho}\left[n_{\text{m}} + n_{\text{n}}\,\frac{\operatorname{Im} b_{\text{n}}(T)}{\operatorname{Im} b_{\text{m}}(T)}\right]\frac{4E_0}{U}\,, \tag{5.11}$$

where n_{n} is the number of hydrogen atoms in an intercrystalline defect, n_{m} is the number of atoms of the main substance in the intercrystalline defect, b_{n} is the mean length of scattering by hydrogen atoms incorporated into the defect, and b_{m} is the mean length of scattering by the atoms of the substance. Thus, the inelastic UCN scattering discovered in experiments [41, 42] can be explained by the enhancement of neutron inelastic scattering by defects containing H_2O or H_2. In this case, the required amount of hydrogen will be much smaller that the value that follows from neutron-optics calculations.

The presence of hydrogen in intercrystalline defects also explains the depolarization of UCNs during storage. Finally, it must be noted that the energy dependences of anomalous and normal UCN losses are different. According to formula (5.3), the energy dependence of normal UCN losses is proportional to $\sqrt{E_0}/\sqrt{U-E_0}$, while that of anomalous UCN losses is proportional to E_0 [according to formula (5.11)]. The difference is due to the different energy dependences of the capture cross section by atoms in coherent scattering and the capture cross section by defects. The dashed curve in Fig. 8 illustrates a fit of the experimental results to the energy dependence of the anomalous UCN loss, i.e., $\mu_{\text{a}} \sim E_0$. Clearly, the experimental findings and the results of the proposed theory of anomalous losses agree. Thus, the developed theory of anomalous neutron losses explains the main features of the phenomenon, namely, the size of losses, their energy dependence, and the paradox concerned with the temperature independence of losses.

Single crystals and amorphous substances with uniform density can be considered exceptions — the effect of anomalous losses under UCN reflection in such substances should be nil. Apparently, frozen LT Fomblin at a temperature close to the solidification point is an example of a substance with very low defect level. Hence, no anomalous losses were discovered for LT Fomblin oil, and the loss factor under UCN reflection (2×10^{-6}) is the smallest among loss factors for all materials studied so far.

A final note concluding this section is in order. The proposed solution to the problem of anomalous neutron losses was done within the framework of ordinary scattering theory. However, the case in question, the subbarrier incoherent scattering at a negative energy ($E_0 - U < 0$), is a rather unique one and has never been considered before.

6. Neutron lifetime measurements using a gravitational UCN trap coated with LT Fomblin oil

6.1 Studying the properties of LT Fomblin trap coatings

In the experiment, a new type of material, low-temperature (LT) Fomblin oil, was used for coating trap walls. This was deposited on the trap surface by evaporation in a vacuum. The oil (Fomblin) contains only C, O, and F, so that the neutron-capture cross section for it is small. As a result of a preliminary study of several types of LT Fomblin it was found [47] that the quasielastic and inelastic UCN scattering in LT Fomblin for $T < -120\,^{\circ}\text{C}$ is much weaker than in ordinary Fomblin at room temperature. Quasielastic UCN scattering is completely suppressed for $T < -120\,^{\circ}\text{C}$ [47], and because of neutron inelastic scattering the expected UCN loss factor η amounts to roughly 2×10^{-6} [48].

The new type of LT Fomblin used in the experiment has a molecular mass $M = 2354$ u and a vapor pressure $P = 1.5 \times 10^{-3}$ mbar at room temperature. Prior to beginning the LT Fomblin deposition procedure, a spherical vaporizer with tiny holes was heated to 140 °C by an electric heater. Then gaseous helium was utilized to force three cubic centimeters of Fomblin oil into the vaporizer's chamber along a vertical tube. The deposition of LT Fomblin amounted to evaporating Fomblin and freezing it, after which it settled on the inner walls of the trap cooled to −150 °C. To achieve homogeneity, the vaporizer was moved up and down.

In order to check the quality of the oil film, a copper trap with a titanium coating was employed. Titanium has a negative scattering length and does not generate a reflecting potential for UCNs. Ultracold neutrons cannot be stored in such a trap if the titanium coating is not covered by a layer of Fomblin. The trap was a 50-cm long cylinder with a diameter of 76 cm. The stable storage time $\tau_{\text{st}} = 869.0 \pm 0.5$ s was achieved after several depositions of LT Fomblin (the total thickness amounted to 15 μm) with the temperature of the trap walls varying from −140 to −150 °C and after a single heating–cooling cycle in which the trap temperature was first raised to room temperature and then brought down to $T = -160\,^{\circ}\text{C}$. Repetition of the thermal cycling had no effect on the UCN storage time in the trap. It is quite possible that at room temperature the oil filled all the gaps and cracks in the trap walls and formed a perfect surface. In addition, LT Fomblin was degassed in the thin layer at room temperature. Such a coating is extremely stable, and no essential variation in the storage time was detected during the eight-day period of

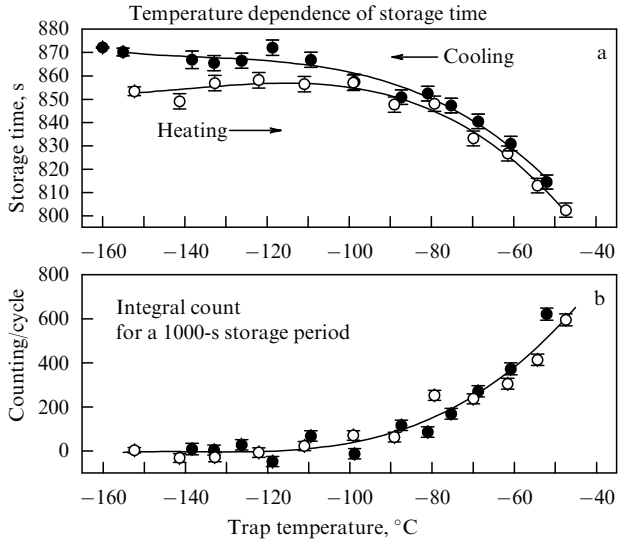

Figure 9. Temperature dependence of (a) the UCN storage time in the course of cooling and heating, and (b) the integral count for a 1000-s storage period.

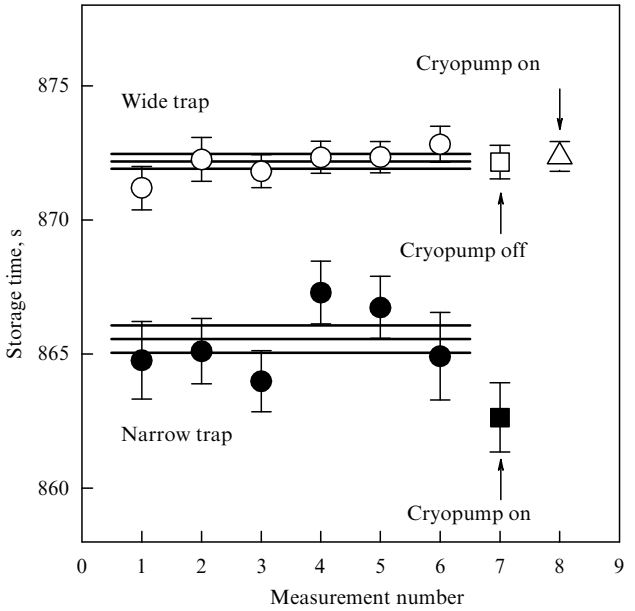

Figure 10. Demonstration of the stability of an LT Fomblin coating during measurements. The UCN storage times for the wide and narrow traps differ because of the different frequencies of UCN collisions with the trap walls.

observation. Subsequent depositions had no effect on the value of the UCN storage time in the trap.

The traps used in the final measurements were coated with beryllium (a quasispherical trap and a narrow cylindrical trap). Since beryllium constitutes a good reflector of ultracold neutrons, the trap walls can be cooled to even lower temperatures, since the appearance of any microcracks in the coating have a small influence on the UCN lifetime in the trap. Using a beryllium-coated trap, we studied the temperature dependence of the storage time for a quasispherical trap coated with LT Fomblin (Fig. 9a).

LT Fomblin oil was frozen on the trap wall at $T = -140\,^{\circ}\mathrm{C}$, then the trap was slowly heated up to $T = -50\,^{\circ}\mathrm{C}$, and finally cooled down again to $T = -160\,^{\circ}\mathrm{C}$. In this way, we covered up the layer defects with oil when it was fairly liquid. After this temperature cycling was completed, the measured storage time turned out to be longer, 872.2 ± 0.3 s, than immediately after sputtering (850 ± 1.8 s). Bearing in mind that the titanium and beryllium traps differed in dimensions, we calculated the difference between the expected and measured storage times for the titanium trap, which was 1.9 ± 0.6 s. This is equivalent to the uncovered part of the surface area of the titanium trap amounting only to $(4.4 \pm 1.3) \times 10^{-7}$. Hence, the reproducible LT Fomblin coating can be obtained irrespective of the material and shape of the trap. For this reason, there is no need to examine the different loss factors η for various traps with a beryllium sublayer under LT Fomblin coating.

In the course of investigations that used a beryllium-coated trap, the quasielastic UCN scattering by LT Fomblin was studied. Figure 9b shows the number of ultracold neutrons that leave the trap during a 1000-s storage period, as a function of the trap temperature. In the process, there was observed an additional (in relation to the background noise) counting rate which fell off exponentially with the passage of the time of UCN storage in the trap. The additional counting rate appears because the UCNs acquire energy in their quasielastic scattering by LT Fomblin. These neutrons leave the trap, which drives the counting rate at the detector up. The counting of quasielastically scattered UCNs becomes indistinguishable against the background (i.e., disappears) as $T < -120\,^{\circ}\mathrm{C}$. This result is in qualitative agreement with that of measuring the quasielastic UCN scattering by LT Fomblin, studied in our previous work [47]. Thus, it turned out that for $T < -120\,^{\circ}\mathrm{C}$ quasielastic UCN scattering could be ignored. Our measurements were done at $T = -160\,^{\circ}\mathrm{C}$ to guarantee that quasielastic scattering does not affect the results. The passage to lower temperatures is undesirable because of a decrease in the LT Fomblin's plasticity and, possibly, the formation of cracks in the coating.

The stability and integrity of the coatings on various traps constitute the most important conditions for the use of the size extrapolation method in measuring the neutron lifetime. Therefore, the quality of the LT Fomblin coating was checked many times during measurements. Figure 10 gives eight results of measurements of the neutron storage time for a quasispherical trap, and seven analogous results for a narrow trap. The measurements were carried out after new depositions, heating, and cooling with a subsequent new deposition, etc. After a liquid-helium cryogenic pump was mounted near the storage volume, the trap's vacuum was improved from 5×10^{-6} to 3×10^{-7} mbar. The storage times during the experiment on measuring the neutron lifetime agree, within approximately one second, for the wide trap and, within marginally broader limits, for the narrow trap. This proves that the LT Fomblin coatings are stable and reproducible for various traps.

Thus, basing our reasoning on the assumption that the substances used for coatings in various UCN traps were identical and taking into account the exceptionally high coating properties of a Fomblin oil, for which surface tension is responsible, and the absence of coating degradation, we believe that the same loss factor η can be used for different traps.

The level of statistical accuracy of our experiment agrees with the requirement that the loss factor η within about 5% is

the same for different traps. However, test experiments have convinced us that this requirement is being met with a much higher accuracy.

6.2 Measurement data and extrapolation to the neutron lifetime

Figure 11 presents the results of measurements of the UCN storage times for various energy intervals and different traps (wide and narrow) as a function of the effective collision frequency γ. Extrapolation of all the data to the neutron lifetime yields a value of 877.60 ± 0.65 s at $\chi^2 = 0.95$, which means that combined extrapolation is possible. However, if we build an energy extrapolation for each trap and combine the two results, we get 875.55 ± 1.6 s.

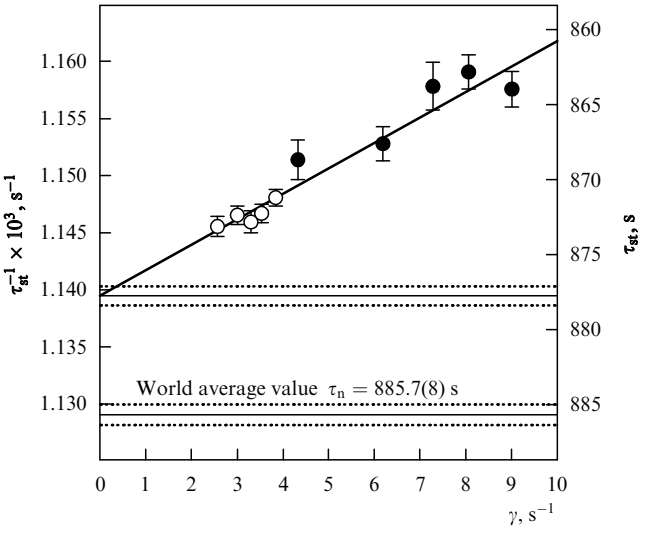

Figure 11. Result of extrapolation to the neutron lifetime when combined energy and size extrapolations are used. The open circles represent the results of measurements for a spherical trap, and the full circles the results of measurements for a cylindrical trap.

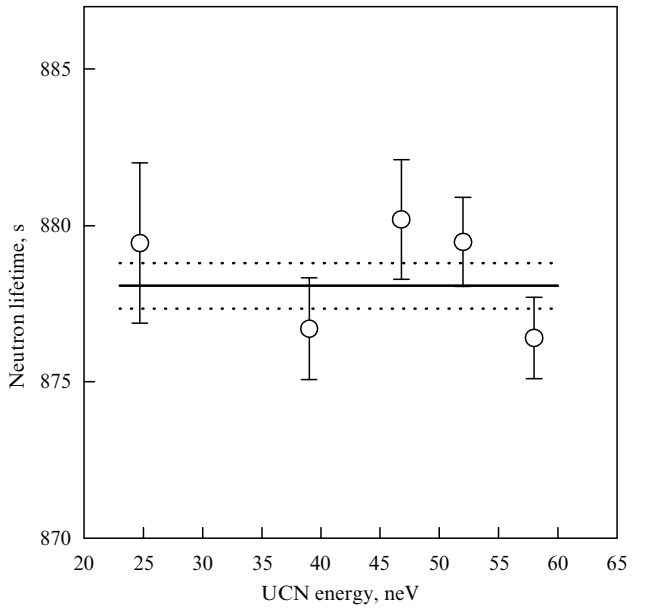

Figure 12. Extrapolated values of the neutron lifetime for different mean UCN energies, when combined energy and size extrapolations are used. The solid straight line corresponds to the average value of neutron lifetime for given measurements.

To use the size extrapolation method, we must combine the values obtained from different traps within the same UCN energy range and then calculate the average value of all the resultant values of the neutron lifetime.

Figure 12 demonstrates the results of size extrapolation to the neutron lifetime for different energy ranges. The average value of the neutron lifetime obtained by the size extrapolation method was 878.07 ± 0.73 s.

The results corresponding to these two methods differ by 1.5σ. The loss factor obtained in this experiment, $\eta = 2 \times 10^{-6}$, agrees with the value found in the transmission experiment [48]. For the final value of the neutron lifetime we prefer using the result of size extrapolation, which depends rather weakly on $\mu(E)$ and which we consider more reliable.

6.3 Monte Carlo simulation of the experiment and systematic errors

To estimate the accuracy and to test the reliability of the size extrapolation method in which the value of the function γ must be calculated, we did a simulation of the experiment by using the Monte Carlo method.

The adopted Monte Carlo model describes the behavior of neutrons with allowance for a gravitational field, the shape of the storage traps, trap losses $\eta = 2 \times 10^{-6}$, and the geometries of the secondary volume and the ultracold neutron guide. As a result, we were able to directly simulate the measurement procedure and to build a time diagram for the counting rate at the detector, similar to the one shown in Fig. 3. The times of UCN storage in traps and the extrapolations to the neutron lifetime that rely on the computed function γ were calculated in the same way as in the experiment. The one adjustable parameter in the Monte Carlo model was the coefficient of UCN diffuse scattering in the interaction with the trap surface. All information about the probability of mirror reflection is extremely important. For instance, if it equals 99.9%, the behavior of UCNs in the trap becomes strongly correlated and predicting the result becomes extremely difficult.

Comparison of the results of Monte Carlo calculations for different values of the diffuse scattering probability and the experimental results (Fig. 13) makes it possible to conclude that the probability of UCN diffuse scattering by the LT Fomblin coating amounts to 10% or more. In Fig. 13a we compare the experimental diagram and the Monte Carlo simulation diagram, obtained with the diffuse scattering coefficients equaling 10% and 100%. The experiment is successfully described for both diffusivity values. However, when the diffuse scattering probability is 0.1%, the agreement between the calculated and experimental results becomes unsatisfactory. The results of such calculations for the first part of the time diagram, which is most sensitive to neutron mirror reflection, are shown on a larger scale in Fig. 13b.

The final simulation of the experiment was done for 10% and 1% diffuse reflection probabilities. The model storage times extrapolated to the neutron lifetime for the wide and narrow cylindrical traps and five different UCN energy ranges are presented in Fig. 14. To simplify the Monte Carlo calculations for the wide trap, we used cylindrical traps instead of quasispherical. In the final analysis of the data obtained with this model, we reproduced the value of the neutron lifetime adopted in the calculation with an accuracy of ± 0.236 s. This accuracy was limited by the statistical

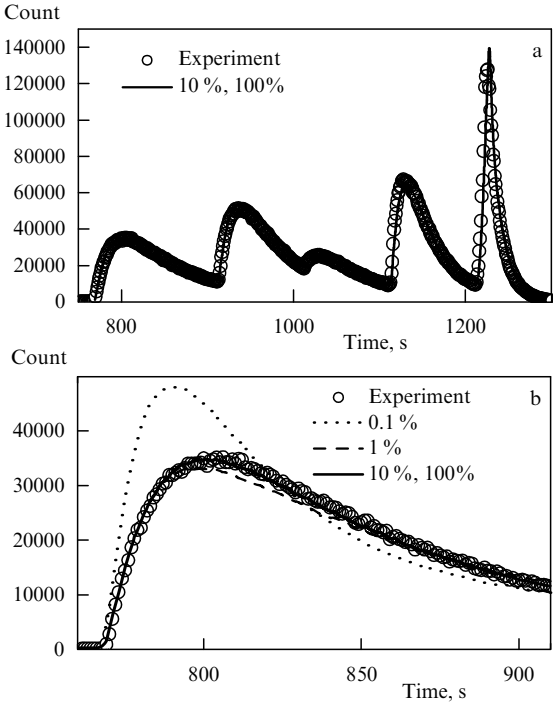

Figure 13. Simulation of an experiment by the Monte Carlo method, consisting in simulating the neutron discharge from a narrow cylindrical trap. The dotted curve corresponds to the results of calculations with a 0.1% diffuse reflection probability; the dashed curve corresponds to a 1% diffuse reflection probability, and the solid curve to 10% and 100%.

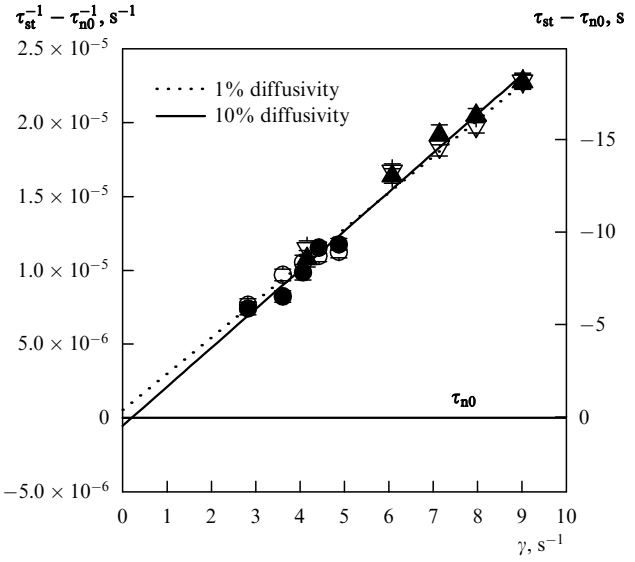

Figure 14. Monte Carlo experiment involving simulation of an extrapolation to the neutron lifetime.

accuracy of the Monte Carlo calculations. Thus, because we employed the computed value of the function γ, the systematic uncertainty of the size extrapolation method amounted to ± 0.236 s.

6.4 Effect of residual gas on UCN storage

When the neutron lifetime is measured with high precision, the effect of residual vacuum on the UCN loss cannot be ignored. For instance, a residual gas pressure of 5×10^{-6} mbar would introduce an error of about 1 s into the value of the UCN lifetime in the trap, which is comparable to the statistical accuracy of the measurements. Such a correction cannot be measured directly (for example, improving a vacuum pressure by an order of magnitude) because the expected effect is smaller than the statistical uncertainty. Instead, we increased the residual gas pressure to 8×10^{-4} mbar. This approach made it possible to measure the parameter $p\tau$ for the residual gas (9.5 mbar s) and obtain the calculated correction to the UCN lifetime in the trap, which amounted to 0.4 ± 0.02 s. This correction does not depend on the UCN energy and can be applied to refining the result for the neutron lifetime.

6.5 The final result for the neutron lifetime and a list of systematic corrections and errors

The magnitudes of the systematic effects and their uncertainties are listed in Table 3.

Table 3. Systematic effects and their uncertainties.

Systematic effect	Magnitude, s	Uncertainty, s
Method of calculating γ	0	0.236
Influence of shape of function $\mu(E)$	0	0.144
UCN spectrum uncertainty	0	0.104
Uncertainty of trap dimensions (1 mm)	0	0.058
Residual gas effect	0.4	0.024
Uncertainty in LT Fomblin critical energy (20 neV)	0	0.004
Total systematic correction	0.4	0.3

The main contribution to the uncertainty is provided by the statistical accuracy of determining the UCN lifetime. The next (by value) uncertainty is that in the calculation of the function γ. The contributions from the uncertainty of the shape of the function $\mu(E)$ and the uncertainty in the UCN spectrum, which are much smaller, were estimated by varying their parameters within the uncertainty limits allowed by the experimental data. Thus, the total systematic correction proved to be equal to 0.4 ± 0.3 s, and the final result for the neutron lifetime amounted to $878.5 \pm 0.7_{stat} \pm 0.3_{sys}$ s.

6.6 Reasons for the discrepancy between the results of experiments on UCN storage

The new result for the neutron lifetime differs from the world average value by 6.5σ, although actually this deviation is determined mainly by the discrepancy between our result and the result of the experiment done by Arzumanov et al. [9], who also achieved high precision in their measurements. It is extremely difficult to discuss the reasons for this discrepancy. We are sure about the results of our experiment, since the probability of UCN losses amounts only to 1% of the probability of neutron β-decay, while in the experiment by Arzumanov et al. [9] the probability of UCN losses amounts to about 30%.

In our experiment, we used solid LT Fomblin, and the process of neutron quasielastic scattering was completely suppressed. Unfortunately, the experiment by Arzumanov et al. [9] was carried out before the effect of quasielastic scattering by liquid Fomblin was discovered, and at present the authors of Ref. [9] are thoroughly analyzing the effect of quasielastic scattering on experimental results.

We are forced to note that in all the experiments involving liquid Fomblin [9, 22, 24], neutron quasielastic scattering was revealed and the process was found to change the spectrum during UCN storage. Although these experiments were run in the scaling mode, i.e., for traps of different dimensions the neutron containment time was chosen in such a way that the number of collisions was the same, the effect of spectrum change caused by quasielastic scattering was not taken into account. Analysis shows that this effect may lead to an overestimated value of the neutron lifetime extrapolated. Finally, our previous experiment may have produced a somewhat overvalued result because of the possible contribution of anomalous losses with a different energy dependence. Although the dependence of the final result on $\mu(E)$ is considerably suppressed when size extrapolation is used, in our previous experiment we used combined extrapolation in which the effect could have been suppressed to a lesser extent. Unfortunately, the level of statistical accuracy of the previous experiment makes an analysis of these assumptions impossible. Furthermore, it must be noted that the coating properties of solid oxygen are inferior to those of Fomblin oil. The portion of the uncoated surface for solid oxygen was approximately 10^{-2}, while that for Fomblin amounted to $(4.4 \pm 1.3) \times 10^{-7}$. The most important problem of the equivalence of the coatings for the wide and narrow traps has been solved more reliably in our recent experiment which uses LT Fomblin.

Thus, our experiment with LT Fomblin possessed a very small loss factor. It also exhibited no effects of anomalous losses and neutron quasielastic scattering, in contrast to other experiments. All this guarantees the reliability of our results.

7. A new result for the neutron lifetime in the Standard Model and in cosmology

7.1 The Standard Model with a new value of τ_n

The new result for the neutron lifetime can be used to test the unitarity of the quark mixing matrix. Figure 15 depicts the dependence of V_{ud} on $-G_A/G_V$, taken from Ref. [1], with allowance for the new result for the neutron lifetime.

The new result for the neutron lifetime differs from the world average value by 6.5σ, and by 5.6σ from the previous most exact result [9]. However, the new result for the neutron lifetime together with the current magnitude of β-asymmetry in the neutron decay ($A_0 = -0.1189\,(7)$ [6]) is in good agreement with the Standard Model.

Note that the result by Abele et al. [6] [$A_0 = -0.1189(7)$] for the β-asymmetry in the neutron decay is more exact in relation to the world average data on β-asymmetry; besides, in Ref. [1] this result was considered the must accurate one, so that it is advisable to use exactly this one.

The matrix element V_{ud} calculated by formula (1.3) with the new neutron lifetime $878.5 \pm 0.7_{stat} \pm 0.3_{sys}$ s and with $\lambda = -1.2739(19)$ (calculated from the value of $A_0 = -0.1189\,(7)$ [6]) is given by

$$V_{ud} = 0.9757 \pm 0.0013\,. \tag{7.1}$$

Test of the unitarity of the first row in the CKM matrix with $V_{us} = 0.2250(27)$ [7] and $V_{ub} = 0.0037(5)$ [7] yields

$$|V_{ud}|^2 + |V_{us}|^2 + |V_{ub}|^2 = 1 - \Delta = 1.0002(27)\,, \tag{7.2}$$

where $\Delta = -0.0002(27) = -0.1\sigma$.

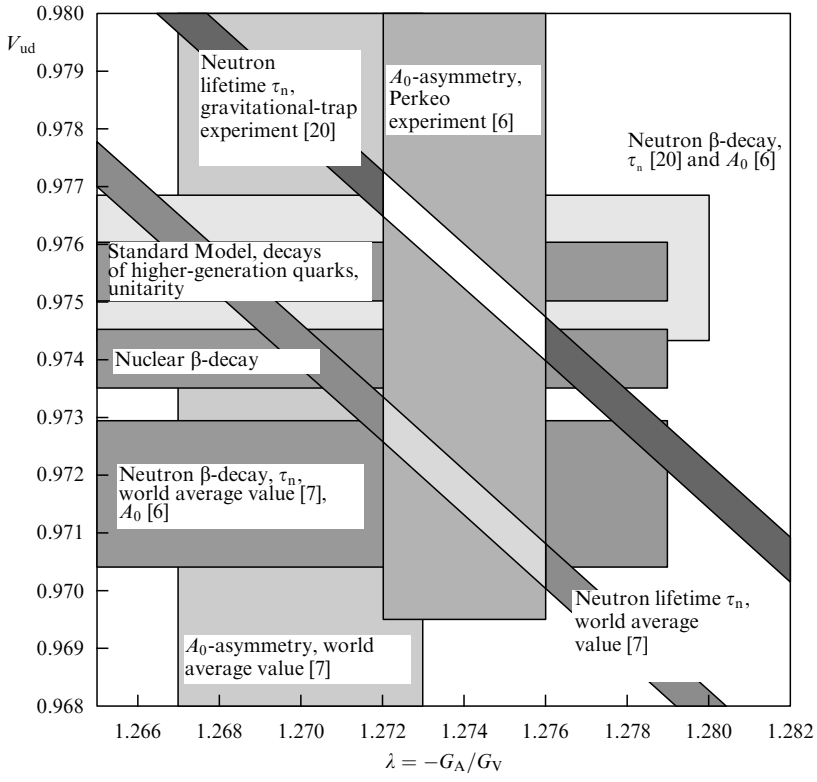

Figure 15. Dependence of the quark-mixing matrix element $|V_{ud}|$ on the ratio of the axial weak coupling constant to the vector weak coupling constant. The values of $|V_{ud}|$ were obtained from various experimental results: from decays of higher-generation quarks and unitarity, from *ft* nuclear decays, and from neutron β-decay.

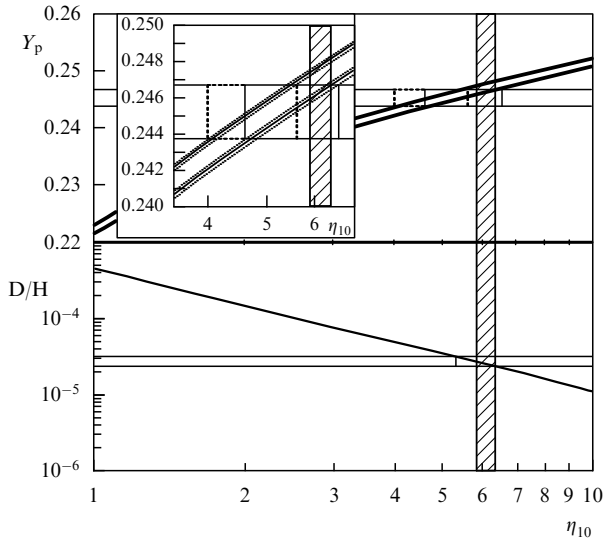

Figure 16. The predicted abundance of low-Z elements in the nucleosynthesis in the Big Bang as a function of the baryon-to-photon ratio η_{10}. The abundance values are compared with those obtained from the initial abundance of low-Z elements (horizontal lines) and from an independent source of data on η_{10} obtained from the results of observations of cosmic background maps (the vertical hatched region). The inset shows on a larger scale the region where the data intersect. The upper heavy line is constructed on the basis of the world average value $\tau_n = 885.7 \pm 0.8$ s; its thickness represents the error corridor in determining τ_n. The lower heavy line is constructed on the basis of the new measurements, $\tau_n = 878.5 \pm 0.8$ s; its thickness also represents the error corridor in determining τ_n. The previous region of allowed values of η_{10} (the rectangle with dashed sides) is shifted into the rectangle with solid sides if the new value of the neutron lifetime is used.

Thus, the new result for the neutron lifetime eliminates the emerging deviation from the unitarity of the quark mixing matrix and confirms the validity of the Standard Model.

7.2 Nucleosynthesis in the Big Bang with a new value of τ_n

Detailed analysis of the nucleosynthesis process in the early stages of the formation of the Universe was recently made by Mathews et al. [15]. They analyzed the effect of the new value of the neutron lifetime on the consistency of data on the initial abundances of D and ^{4}He isotopes and the data on baryon asymmetry η_{10}. Figure 16 displays the dependences of the initial abundance of ^{4}He (Y_p) and deuterium (D/H) on the baryon asymmetry η_{10} taken from Ref. [15].

Clearly, the use of the new value of the neutron lifetime improves the agreement between the data on the initial abundances of deuterium and helium, and those on baryon asymmetry. Although the accuracy of the cosmological data is much lower than that of measurements of the neutron lifetime, the shift of τ_n from the world average value to the new value has a certain effect on the verification of the nucleosynthesis model in the early stages of the formation of the Universe.

8. The prospects of precision studies of neutron β-decay

Before concluding the review and stating that the Standard Model has again proved to be valid, let us examine the prospects for further studies and chances of going beyond the Standard Model.

Of course, the next important step that must be taken in precision studies of neutron β-decay is to measure the decay asymmetry A_0 with a relative accuracy of 10^{-3}. Only after such accuracy is achieved can we say that the region where the data on τ_n and A_0 intersect in Fig. 15 corresponds to the accuracy of the data on $V_{ud} = \sqrt{1 - V_{us}^2}$, i.e., an accuracy that follows from the unitarity of the CKM matrix and the data on strange particle decay. First, the accuracy in testing the unitarity of the CKM matrix will then increase by a factor of four to five and will be determined, to the same extent, by the accuracy of experimental measurement, as well as by the accuracy of calculations of the internal radiative corrections. Second, precise measurements of the β-decay asymmetry are the source of entirely new information related to the axial weak coupling constant, in contrast to measurements of $f\tau_{00}$, in which only the vector constant G_V is involved. In particular, the admixture of the (V + A) variant of coupling to the standard (V − A) variant of coupling immediately reduces the asymmetry of the decay, both the electron asymmetry A_0 and the neutrino asymmetry B_0. The presence of right-handed currents, i.e., the (V + A) variant of coupling, may be detected by analyzing the difference between the experimentally found value A_{exp} and the asymmetry calculated within the V − A theory with the use of the ratio λ_{n-00} obtained as result of intersection of the 'neutron-lifetime' and 'nuclear-β-decay' straight lines in Fig. 15. This difference in asymmetries can be shown (see Refs [59, 60]) to be related to the parameters of the simplest left–right weak interaction model, δ and ζ, in the following manner:

$$A_{exp} - A(\lambda_{n-00}) = 0.23\,\delta^2 + 2.2\,\delta\zeta + 1.1\zeta^2,$$

$$B(\lambda_{n-00}) - B_{expt} = 1.95\,\delta^2 + 2.2\,\delta\zeta + 1.1\,\zeta^2,$$

where δ is the ratio of the squares of the masses of the left (W_L) and right (W_R) vector bosons, and ζ is their mixing angle. An example of such analysis can be given if we use the world average experimental values of A_0, B_0, λ_{n-00} extracted from $f\tau_n$ and $f\tau_{00}$: here, $A_{exp} - A(\lambda_{n-00}) = 0.23\,\delta^2 + 2.2\,\delta\zeta + 1.1\,\zeta^2 = 2.1\,\sigma$ and $B(\lambda_{n-00}) - B_{expt} = 1.95\,\delta^2 + 2.2\,\delta\zeta + 1.1\,\zeta^2 = 1.2\sigma$. These values cannot be taken seriously; they serve only as an example of possible analysis. This analysis is exemplified in Fig. 17.

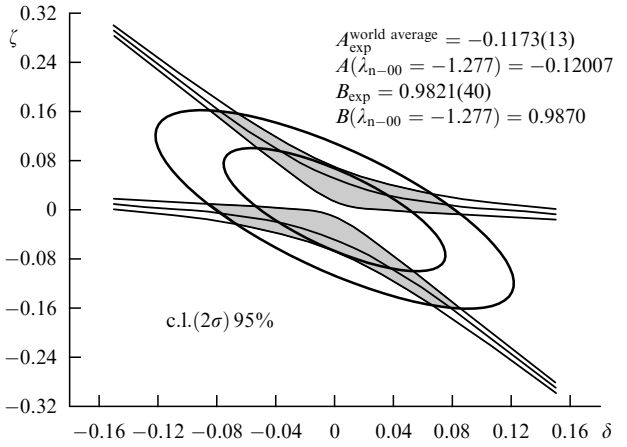

Figure 17. Analysis of experimental data within the simplest left–right weak interaction model (δ is the ratio of the squares of the masses of the left- and right-handed vector bosons, and ζ is their mixing angle). The shaded areas indicate the regions of allowed values of δ and ζ.

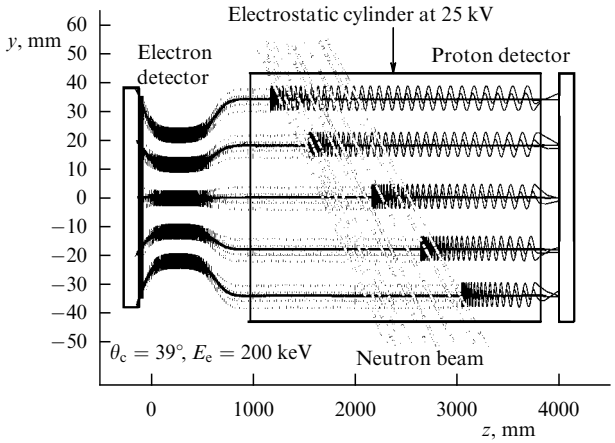

Figure 18. Schematic of the experiment for measuring A_0 and B_0, the configuration of the magnetic field in the correlation spectrometer, and electron and proton trajectories (the scales along the y- and z-axes differ by a factor of 30).

Thus, a further increase in the accuracy of measurements of the β-decay asymmetries is basically important both from the viewpoint of raising the accuracy in testing the unitarity of the CKM matrix and from the viewpoint of searching for possible deviations from the Standard Model.

The schematic sketch of the experiment that is in the preliminary stage at PNPI and will be used to measure A_0 and B_0 with a relative accuracy of one part in a thousand is shown in Fig. 18 [61]. We propose utilizing a polarized beam of cold neutrons and an axial bottle-shaped magnetic field generated by a superconducting solenoid. Such a configuration of the magnetic field makes it possible to isolate the decay electrons within a solid angle determined with high accuracy. The electrostatic cylinder with a potential of 25 kV isolates the region of decays being detected. The protons that have left this region are accelerated and detected by a proton counter. The use of counter pulse coincidences of electron and proton signals substantially suppresses background noise. The asymmetry of electron ejection in relation to the neutron spin is measured by the changes in the sign of polarization of the neutron beam. The final accuracy of the decay asymmetry will be determined by the accuracy of polarization measurements, which amounts to $(1-2)\times 10^{-3}$ [62, 63]. Figure 18 shows the configurations of the magnetic field and the trajectories of the electrons and protons traveling along the magnetic field intensity lines to the detectors. Only the electrons that were ejected within the solid angle $\theta_c \approx 39°$, which is determined by the ratio of the magnetic field intensity in the uniform region (H_0) to that in the magnetic mirror (H_m), $\sin^2\theta_c = H_0/H_m$, reach the electron counter. The neutron beam will pass through the superconducting solenoid at a small angle to the solenoid's axis ($\sim 5°$), which guarantees a large path length for the neutrons and boosts the statistics of the neutron decays recorded. So far, pilot experiments have been conducted, and they suggest that it is possible to achieve a relative accuracy of one part in a thousand in measuring A_0 and B_0.

In conclusion, it should be remarked that in both Europe and the United States new precise experiments on measuring the neutron lifetime and the decay asymmetries are being planned. Apparently, in the next five years research in this field will be much more intense and we will find the answer, at a new level of accuracy, to the problem of the status of the Standard Model in analyzing the data on neutron β-decay.

9. Commentary

The present review, which is based on earlier published works, summarizes the research done in order to obtain the most precise value of the neutron lifetime and to solve the problem of anomalous UCN losses. The series of investigations discussed here was carried out by the staff of the Laboratory of Neutron Physics at the Petersburg Nuclear Physics Institute, Gatchina comprising A G Kharitonov, V E Varlamov, A K Fomin, M S Lasakov, R R Tal'daev, A V Vasil'ev, E V Siber, S O Sumbaev, N V Romanenko, O M Zherebtsov, and some others. Other departments of the Institute and the staff of the VVR-M reactor also significantly contributed to this research.

A substantial contribution to building the experimental facility for measuring the neutron lifetime was provided by colleagues at JINR, Dubna: V P Alfimenkov, A V Strelkov, V N Shvetsov, V I Lushchikov, and some others.

In our experiments held at ILL, Grenoble invaluable assistance was provided by P Geltenbort and T Brenner, and also by the staff of the ILL reactor.

The research into the properties of low-temperature Fomblin done by Yu N Pokotilovskii (JINR), which involved using cold-neutron beams, played an important role in selecting the optimal coating for the UCN trap.

Finally, I would like to mention the help provided by the staff of the Paul Scherrer Institute (Switzerland) and the University of Rhode Island (USA).

To a great extent, the experiments were made possible by the support of the Elementary Particle Physics program of the Russian Academy of Sciences, and the Russian Foundation for Basic Research (grants Nos 99-02-16621 and 04-02-17440).

References

1. Abele H et al. *Eur. Phys. J. C* **33** 1 (2004)
2. Wilkinson D H *Nucl. Phys. A* **377** 474 (1982)
3. Gzarnecki A, Marciano W, Sirlin A, Preprint (in preparation)
4. Towner I S *Nucl. Phys. A* **540** 478 (1992)
5. Towner I S, Hardy J C *J. Phys. G: Nucl. Part. Phys.* **29** 197 (2003)
6. Abele H et al. *Phys. Rev. Lett.* **88** 211801 (2002)
7. Particle Data Group: Eidelman S et al. *Phys. Lett. B* **592** 1 (2004)
8. Sher A et al. *Phys. Rev. Lett.* **91** 261802 (2003); hep-ex/0305042
9. Arzumanov S et al. *Phys. Lett. B* **483** 15 (2000)
10. Hagiwara K et al. (Particle Data Group) *Phys. Rev. D* **66** 010001 (2002)
11. Marciano W J, Sirlin A *Phys. Rev. Lett.* **56** 22 (1986)
12. Langacker P, Luo M *Phys. Rev. D* **45** 278 (1992)
13. Marciano W J, Sirlin A *Phys. Rev. D* **35** 1672 (1987)
14. Dentsch I, in *Fundamental Symmetries and Nuclear Structure*: *Tests of Fundamental Symmetries in Nuclei and the Structure of Nuclei as Measured by Medium Energy Probes*: *Proc. of the 2nd Workshop, Santa Fe, NM, USA, October 12, 1988* (Eds J N Ginocchio, S P Rosen) (Singapore: World Scientific, 1989); Holstein B R, Treiman S B *Phys. Rev. D* **16** 2369 (1977)
15. Mathews G J, Kajino T, Shima T *Phys. Rev. D* **71** 021302(R) (2005)
16. Bondarenko L N et al. *Pis'ma Zh. Eksp. Teor. Fiz.* **28** 329 (1978) [*JETP Lett.* **28** 303 (1978)]
17. Christensen C J et al. *Phys. Rev. D* **5** 1628 (1972)
18. Dewey M S et al. *Phys. Rev. Lett.* **91** 152302 (2003)
19. Zel'dovich Ya B *Zh. Eksp. Teor. Fiz.* **36** 1952 (1959) [*Sov. Phys. JETP* **9** 1389 (1959)]
20. Serebrov A et al. *Phys. Lett. B* **605** 72 (2005)
21. Byrne J et al. *Europhys. Lett.* **33** 187 (1996)

22. Mampe W et al. *Pis'ma Zh. Eksp. Teor. Fiz.* **57** 77 (1993) [*JETP Lett.* **57** 82 (1993)]
23. Nesvizhevskii V V et al. *Zh. Eksp. Teor. Fiz.* **102** 740 (1992) [*Sov. Phys. JETP* **75** 405 (1992)]
24. Byrne J et al. *Phys. Rev. Lett.* **65** 289 (1990)
25. Mampe W et al. *Phys. Rev. Lett.* **63** 593 (1989)
26. Kharitonov A G et al. *Nucl. Instrum. Meth. A* **284** 98 (1989)
27. Kossakowski R et al. *Nucl. Phys. A* **503** 473 (1989)
28. Paul W et al. *Z. Phys. C* **45** 25 (1989)
29. Spivak P E *Zh. Eksp. Teor. Fiz.* **94** (9) 1 (1988) [*Sov. Phys. JETP* **67** 1735 (1988)]
30. Last J et al. *Phys. Rev. Lett.* **60** 995 (1988)
31. Arnold M "Messung der Lebensdauer freier Neutronen", Dissertation (Heidelberg: Univ. of Heidelberg, 1987)
32. Kosvintsev Yu Yu, Morozov V I, Terekhov G I *Pis'ma Zh. Eksp. Teor. Fiz.* **44** 444 (1986) [*JETP Lett.* **44** 571 (1986)]
33. Byrne J et al. *Phys. Lett. B* **92** 274 (1980)
34. Ignatovich V K *The Physics of Ultracold Neutrons* (Oxford: Clarendon Press, 1990)
35. Kosvintsev Yu Yu et al. *Pis'ma Zh. Eksp. Teor. Fiz.* **28** 164 (1978) [*JETP Lett.* **28** 153 (1978)]
36. Alfimenkov V P et al. *Pis'ma Zh. Eksp. Teor. Fiz.* **55** 92 (1992) [*JETP Lett.* **55** 84 (1992)]
37. Arzumanov S S et al. *Yad. Fiz.* **66** 1868 (2003) [*Phys. At. Nuclei* **66** 1820 (2003)]
38. Varlamov V E et al. *Zh. Eksp. Teor. Fiz.* **114** 786 (1998) [*JETP* **87** 426 (1998)]
39. Groshev L V et al. *Phys. Lett. B* **34** 293 (1971)
40. Lobashev V M, Porsev G D, Serebrov A P, Preprint LNPI-37 (Gatchina: LNPI, 1973); Egorov A I et al. *Yad. Fiz.* **19** 300 (1974) [*Sov. J. Nucl. Phys.* **19** 147 (1974)]
41. Strelkov A V, Hetzelt M *Zh. Eksp. Teor. Fiz.* **74** 23 (1978) [*Sov. Phys. JETP* **47** 11 (1978)]
42. Zhukov S V et al. *Pis'ma Zh. Eksp. Teor. Fiz.* **57** 446 (1993) [*JETP Lett.* **57** 464 (1993)]
43. Bates J C *Phys. Lett. A* **88** 427 (1982)
44. Ageron P, Mampe W, Kilvington A I *Z. Phys. B* **59** 261 (1985)
45. Bondarenko L N et al. *Yad. Fiz.* **65** 13 (2002) [*Phys. At. Nuclei* **65** 11 (2002)]
46. Serebrov A P et al. *Phys. Lett. A* **309** 218 (2003)
47. Steyerl A et al. *Eur. Phys. J. B* **28** 299 (2002)
48. Pokotilovskii Yu N *Zh. Eksp. Teor. Fiz.* **123** 203 (2003) [*JETP* **96** 172 (2003)]
49. Ignatovich V K, Satarov L M, Preprint No. 2820 (Moscow: Institute of Atomic Energy, 1977)
50. Lychagin E V et al. *Yad. Fiz.* **65** 2052 (2002) [*Phys. At. Nuclei* **65** 1995 (2002)]
51. Serebrov A, Preprint PNPI-2193 (Gatchina: PNPI, 1997)
52. Serebrov A, Romanenko N, Preprint PNPI-2194 (Gatchina: PNPI, 1997)
53. Serebrov A et al. *Phys. Lett. A* **335** 327 (2005)
54. Serebrov A et al. *Nucl. Instrum. Meth. A* **440** 717 (2000)
55. Serebrov A P et al. *Phys. Lett. A* **313** 373 (2003)
56. Varlamov V E et al. *Pis'ma Zh. Eksp. Teor. Fiz.* **66** 317 (1997) [*JETP Lett.* **66** 336 (1997)]
57. Golub R, Richardson D J, Lamoreaux S K *Ultra-Cold Neutrons* (Bristol: A. Hilger, 1991)
58. Lax M *Rev. Mod. Phys.* **23** 287 (1951)
59. Holstein B R, Treiman S B *Phys. Rev. D* **16** 2369 (1977)
60. Serebrov A P, Romanenko N V *Pis'ma Zh. Eksp. Teor. Fiz.* **55** 490 (1992) [*JETP Lett.* **55** 503 (1992)]
61. Serebrov A et al., Preprint PNPI-2572 (Gatchina: PNPI, 2004)
62. Serebrov A P et al. *Nucl. Instrum. Meth. A* **357** 503 (1995)
63. Zimmer O et al. *Nucl. Instrum. Meth. A* **440** 764 (2000)